Generalized Operational Short-Circuit Ratio for Grid Strength Assessment in Power Systems with High Renewable Penetration

Chenxi Liu, Huanhai Xin, Di Wu, Huisheng Gao, Hui Yuan, Yuhan Zhou

***Abstract*— The growing integration of converter-interfaced generators (CIGs) has caused small-signal stability issues driven by the converter control interaction of CIGs, especially in weak grids. Grid strength assessment is an important tool for fast identifying the stability issues. However, the existing techniques are ineffective in a multi-CIG system under actual operating conditions (MCIGS-AO). It is challenging for the small-signal stability analysis in a MCIGS-AO while considering different terminal voltages and power outputs for CIGs coupled with their different control parameters and configurations. The black-box converter modeling further increases the analysis complexity. This paper proposes a method for fast identifying the small-signal stability issues in a MCIGS-AO via grid strength assessment. First, we leverage the multiple-time scale analysis technique to study converter control dynamics with a focus on the stability issues mainly caused by converter phase-lock loops. Then, we transform a MCIGS-AO into a set of simple subsystems for the small-signal stability analysis. According to the analysis results, we propose the generalized operational short-circuit ratio (gOSCR) and critical gOSCR (i.e., CgOSCR) to assess grid strength in terms of the small-signal stability. With the gOSCR and CgOSCR, our method is proposed, and it is applicable even when converter details are unknown. The proposed method is validated on a modified IEEE 39-bus system and a practical power system with high wind generation.**

***Index Terms*—Small-signal stability, grid strength, actual operating conditions, short-circuit ratio.**

I. Introduction

The increasing penetration of renewable energy resources into the electric power grid through power electronic converters has changed grid dynamics [1]-[5] and caused new types of small-signal stability issues, such as issues resulting from the interaction between fast-acting converter controls of converter-interfaced generators (CIGs) [3]-[11]. Particularly, the small-signal stability issues become prominent in weak grids.

Grid strength assessment is an important tool for fast identifying small-signal stability issues [12]-[23]. Various methods have been developed to quantify grid strength. Short-circuit ratio (SCR) is an index recommended by North American Electric Reliability Corporation[12]. However, the SCR is effective only for investigating a single CIG; the SCR cannot handle interactions between multiple CIGs. To overcome this limitation, different indices have been proposed based on either engineering experience or theoretical derivations. The former includes the weighted SCR (WSCR) [15], the composite SCR (CSCR) [16], the equivalent SCR (ESCR) [17], the SCR with interaction factors (SCRIF) [18]; the latter comprises the generalized SCR (gSCR) [19]-[21] and the hybrid multi-infeed interactive effective SCR (HMIESCR) [22][23].

The existing methods are mainly developed based on rated operating conditions (e.g., rated CIG capacity and rated terminal voltage). However, the small-signal stability issues are dependent on the actual operating conditions [17][18]. The actual active power outputs and terminal voltages of CIGs often deviate from the rated values and differ from each other. Thus, the existing methods may be invalid or even provide misleading assessment results for identifying small-signal stability issues in a multi-CIG system under actual operating conditions (MCIGS-AO).

To overcome the limitation, it needs to address two major challenges for the small-signal stability analysis in a MCIGS-AO. First, a practical MCIGS-AO is a heterogeneous system where converters have different control configurations and parameters. The heterogeneity becomes more significant when considering different terminal voltages and active power outputs for CIGs coupled with their different converter control. In such a MCIGS-AO, it is challenging to analyze the small-signal stability for developing an effective method for grid strength assessment. Second, the analysis becomes more complex when converter details are unknown due to the intelligent property concern of converter vendors.

By addressing the two challenges, this paper presents a method for fast identifying the small-signal stability issues in a MCIGS-AO. First, the multi-time scale analysis technique is used to study the converter control dynamics. Then, a MCIGS-AO is transformed into a set of subsystems for the small-signal stability analysis. Based on the analysis results, we define the generalized operational short-circuit ratio (gOSCR) and critical gOSCR(i.e., CgOSCR) for grid strength assessment in terms of small-signal stability in a MCIGS-AO. With the gOSCR and CgOSCR, our method is proposed to fast identify the small-signal stability issues in a MCIGS-AO. The major contributions of the proposed method are summarized below:

This work was jointly supported by the National Natural Science Foundation of China (No.U2166204, U22B6008) and supported in part by the National Science Foundation Award 2033355.

Chenxi Liu, Huanhai Xin, Huisheng Gao, HuiYuan, and Yuhan Zhou are with the college of electrical engineering, Zhejiang university, Hangzhou 310027, China (Emails: {12010046, xinhh, 11610051, gaohuisheng, zhouyuhan}@zju.edu.cn); (*Corresponding author: Huanhai Xin*).

D. Wu is with the department of electrical and computer engineering, North Dakota State University, Fargo, 58102, USA. (Emails: di.wu.3@ndsu.edu).

1) By the multi-time scale analysis for converter control dynamics with a focus on the stability issues mainly caused by converter phase-lock loops(PLLs), we first decouple converter control dynamics from actual operating conditions and then transform a MCIGS-AO into a set of subsystems for the small-signal stability analysis.
2) Based on the analysis results, the gOSCR is defined to quantify grid strength in terms of small-signal stability while CgOSCR is defined as the threshold of the gOSCR and thus gOSCR=CgOSCR can characterize the system stability boundary. Moreover, an analytical expression is derived to evaluate the CgOSCR under actual operating conditions. This analytical expression allows us to avoid a trial-and-error approach based on electromagnetic transient simulations to determine the CgOSCR, even when the converters are represented by black-box models. Furthermore, this expression provides the theoretical foundations to explore insights into the impact on the system stability boundary due to various factors such as actual operating conditions, converter control parameters and configurations, and network structure.
3) With the gOSCR and CgOSCR, a method is proposed for fast identifying the small-signal stability issues and the system stability margin in a MCIGS-AO. The method is applicable for a practical power system with high CIG penetration, even when converter details are unknown.

The rest of this paper is organized as follows. In Section II, we elaborate on the challenges to assessing grid strength in terms of small-signal stability in a MCIGS-AO. In Section III, we formulate the modeling of a MCIGS-AO. Then, we analyze the small-signal stability of MCIGS-AO in Section IV. In Section V, the gOSCR and CgOSCR are defined and a method is proposed for assessing grid strength to identify small-signal stability issues in a heterogeneous MCIGS-AO. In Section VI, the implementation of the proposed method is discussed. In Section VII, the proposed method is verified on a modified IEEE 39-bus system and a practical power system with high wind generation via modal analysis and electromagnetic transient simulations. Section VIII concludes the paper.

II. Problem Statement

Grid strength assessment is a useful tool for fast identifying the small-signal stability issues resulting from the converter control interaction in a power system with high CIG penetration. In the literature, however, the existing techniques are mainly developed based on the rated operating conditions. Thus, they may be invalid or even provide misleading assessment results for identifying small-signal stability issues under actual operating conditions.

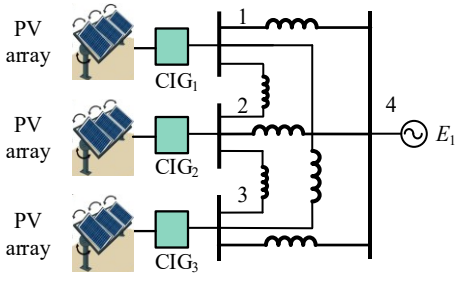

(a) The three-converter system.

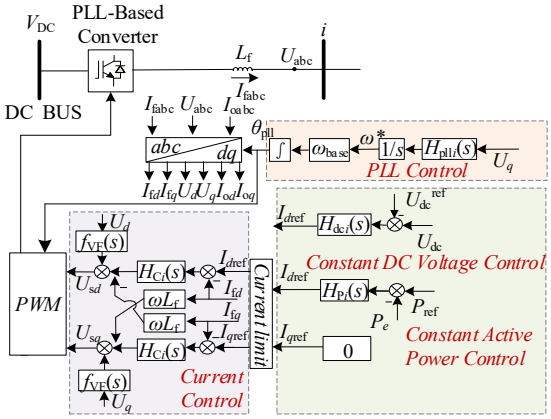

(b) The CIG control structure.

Fig. 1 Illustration of the three-converter system with CIG control structure.

To illustrate this concern, let us look at a three-converter system as shown in Fig. 1. The converter control parameters and network parameters can be found in TABLE A. I of Appendix A. In the system, under the actual operating conditions presented in TABLE I, a small disturbance is applied to bus 4 at 0.20s to cause the voltage to rise by 5% and then is cleared at 0.25s. While all buses 1~3 have divergent voltage oscillations following this disturbance, divergent voltage oscillation at bus 3 is significant. Fig. 2 shows the voltage trajectories at converter terminal bus 3. This indicates the system loses its stability following this disturbance.

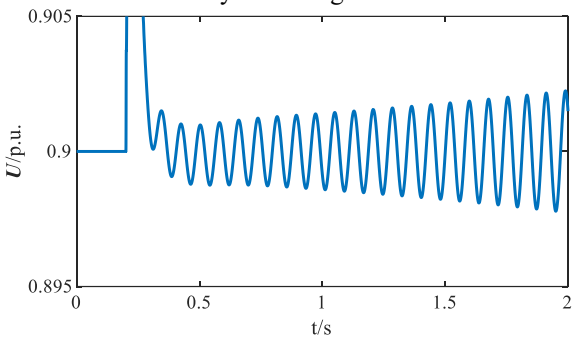

Fig. 2 Trajectories of the terminal voltage at bus 3 in the three-converter system under the actual operating conditions.

It is expected that the existing techniques can identify the small-signal instability issue as shown in Fig. 2. However, they provide misleading identification results under the actual operating conditions. Without the loss of generality, we select three typical indices for this illustration. These indices are SCR [12], ESCR [17], and gSCR [21]. Since SCR and ESCR are bus-wise indices, we use the minimum of SCR_i and $ESCR_i$, at buses i=1,2,3 to describe the strength of the entire system. The gSCR is the system-wise index, so its evaluation result can directly characterize the strength of the entire system. TABLE II presents the evaluation results of these indices and their thresholds. The threshold for gSCR is calculated based on the method presented in [21]. It can be seen from TABLE II that the evaluation results of all these indices suggest that the system under the actual operating conditions is strong, so there should not be any system instability issues following the disturbance. But the results are contrary to the observation from Fig. 2.

TABLE I
TERMINAL VOLTAGES, ACTIVE POWER OUTPUTS, AND CURRENT OUTPUTS OF THREE CONVERTERS UNDER THE ACTUAL OPERATING CONDITIONS(PER-UNIT).

Bus	1	2	3
U/p.u.	0.95	0.92	0.90
P/p.u.	0.20	0.80	1.00
I/p.u.	0.21	0.87	1.11

TABLE II
EVALUATION RESULTS OF SCR, ESCR, GSCR, AND THEIR THRESHOLDS

Indices	SCR	ESCR	gSCR [21]
Values	3.88	3.16	3.70
Thresholds	3[13]	3[18]	3.64
System Stability Identification	3.88>3 Stable	3.16>3 Stable	3.70>3.64 Stable
	Contrary to the identification results obtained from the electromagnetic transient simulation		

Due to the following shortcomings, SCR, ESCR, and gSCR provide misleading identification results under actual operating conditions:

1) In the system, the small-signal stability depends on actual operating conditions, which often deviate from the rated active power output and rated terminal voltage of CIGs. However, SCR, ESCR, and gSCR are defined based on rated operating conditions, so they cannot accurately assess system stability in a MCIGS-AO. Moreover, ESCR is defined based on engineering experience and thus lacks theoretical justification for assessing system stability in a multi-CIG system under rated operating conditions. SCR is only effective in a grid-tied single CIG system.
2) To identify the small-signal instability issues using these indices, it needs to compare these indices with their thresholds. However, the thresholds of SCR and ESCR are usually determined based on engineering experience without considering actual operating conditions[13][18]. The threshold for gSCR is determined by an analytical expression, but it is also derived based on the rated operating conditions[21].

To overcome these shortcomings, it needs to address the following challenges.

1) To overcome the aforementioned shortcoming 1), it is important to understand the small-signal stability of a MCIGS-AO. However, various operating conditions coupled with different control parameters and configurations significantly increase the complexity of small-signal stability analysis. For example, in the three-converter system in Fig. 1, each converter can be modeled by its $\boldsymbol{Y}_{\mathrm{CIG}i}(s)$ in (1) (i=1,2,3). These three converters have different current outputs and terminal bus voltages, I_1=0.21, I_2=0.87, I_3=1.11, U_1=0.95, U_2=0.92, U_3=0.90. The different operating conditions lead to a heterogeneous three-converter system, even though these three converters have the same control configuration and parameters. When converters have different control configurations and parameters coupled with different actual operating conditions, it becomes more difficult for the stability analysis in the system.

$$\boldsymbol{Y}_{\mathrm{CIG}i}(s)=\begin{bmatrix} Y_{g11i}(s) & Y_{g12i}(s) \\ Y_{g21i}(s) & Y_{g22i}(s) \end{bmatrix} \tag{1}$$

$$\begin{cases} Y_{g11i}(s)=\dfrac{\left(1-f_{VF}(s)\right)+H_{Ci}(s)G_{\mathrm{APC}i}(s)I_i}{sL_{\mathrm{f}}+H_{Ci}(s)+H_{Ci}(s)G_{\mathrm{APC}i}(s)U_i} \\ Y_{g12i}(s)=Y_{g21i}(s)=0 \\ Y_{g22i}(s)=\dfrac{\left(1-f_{VF}(s)\right)-H_{\mathrm{pll}i}(s)H_{Ci}(s)I_i}{\left(1+U_iH_{\mathrm{pll}i}(s)\right)\left(sL_{\mathrm{f}}+H_{Ci}(s)\right)} \end{cases}$$

2) To overcome the shortcoming 2), it needs to determine the threshold under actual operating conditions. However, the control structure and/or parameters of CIGs may be unknown due to the intelligent property concern of converter vendors. This not only increases the difficulty of the small-signal stability analysis, but it is also challenging for deriving an analytical expression to determine the threshold in order to avoid a trial-and-error approach based on electromagnetic transient simulations. For example, for the converter in the three-converter system, it can be modeled by $\boldsymbol{Y}_{\mathrm{CIG}i}(s)$ in (1). When converter details are not disclosed, $H_{Ci}(s)$, $H_{\mathrm{pll}i}(s)$, $f_{\mathrm{VF}}(s)$, and $G_{\mathrm{APC}i}(s)$ in (1) are unknown, which makes it hard to analytically determine the threshold and theoretically analyze the small-signal stability due to converter control parameters coupled with actual operating conditions.

In the following sections of this paper, we will address the challenges of developing a grid strength assessment method for identifying the small-signal stability issues in a MCIGS-AO.

III. MODELING MCIGS-AO

Let us consider a MCIGS-AO with n CIGs as shown in Fig. 3, where buses 1, ..., n are connected to n CIGs with different control configurations (e.g., the outer loop control adopts the constant active power control loop or constant DC voltage control loop), control parameters, and actual operating conditions (e.g., different active power outputs and terminal voltages for CIGs); buses n+1, ..., n+m are passive buses that are not connected to either CIGs or voltage sources; and bus n+m+1 is the infinite bus, which is connected to the voltage source. Since the majority of current CIGs are interfaced with practical power grids through grid-following converters using a PLL for grid synchronization, we consider all n CIGs are integrated into the system through grid-following converters [24]-[26]. The power factor of each CIG is assumed to be 1 since the majority of CIGs such as wind and solar currently integrated into practical power grids work with high power factor close to 1[27][28].

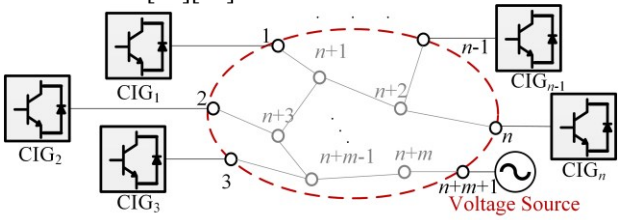

Fig. 3. Illustration of the studied MCIGS-AO.

According to multiple-scale analysis in [29], it is known that the fast (short timescale) and slow (long timescale) dynamics of a system are almost independent provided that their timescales are sufficiently separated. For the multi-time scale converter control in a CIG [29], we separate slow control dynamics from fast converter control dynamics for the small-signal stability analysis of the heterogeneous MCIGS-AO. Particularly, this paper focuses on the small-signal stability issues mainly caused by PLLs. Since PLLs are in the medium frequency band [6]-[9], the following two approximations are considered in the modeling for the MCIGS-AO.

Approximation 1: The voltage feedforward filter is ignored since its bandwidth is in the high-frequency band.

Approximation 2: The fast dynamics of the current control loop can be ignored since the response speed of PLLs is much lower than the current control loop.

Due to the intelligent property concern of vendors, the control structure and parameters of CIGs may be unknown. This increases the difficulty of the small-signal stability analysis in a MCIGS-AO, especially when considering different actual operating conditions coupled with different converter control parameters and configurations. To address this challenge, we will model the MCIGS-AO based on the admittance modeling, which allows us to measure the admittance of CIGs without needing the converter details. This admittance modeling for the MCIGS-AO includes linearized equations for CIGs and the power network, respectively.

A. CIG Modeling

For each CIG in the MCIGS-AO as shown in Fig. 1, its admittance model $\boldsymbol{Y}_{\mathrm{CIG}i}(s)$ can be generally represented below [30]. The admittance models for n CIGs are different, due to different actual operating conditions, control parameters, and configurations for CIGs.

$$\begin{bmatrix}\Delta I_{ix}\\ \Delta I_{iy}\end{bmatrix}=\underbrace{\begin{bmatrix}Y_{g11i}(s) & Y_{g12i}(s)\\ Y_{g21i}(s) & Y_{g22i}(s)\end{bmatrix}}_{\boldsymbol{Y}_{\mathrm{CIG}i}(s)}\begin{bmatrix}\Delta U_{ix}\\ \Delta U_{iy}\end{bmatrix} \tag{2}$$

$$\begin{cases}Y_{g11i}(s)=\dfrac{\left(1-f_{VF}(s)\right)+H_{\mathrm{C}i}(s)G_{\mathrm{APC}i}(s)I_i}{sL_{\mathrm{f}}+H_{\mathrm{C}i}(s)+H_{\mathrm{C}i}(s)G_{\mathrm{APC}i}(s)U_i}\\ Y_{g12i}(s)=Y_{g21i}(s)=0\\ Y_{g22i}(s)=\dfrac{\left(1-f_{VF}(s)\right)-H_{\mathrm{pll}i}(s)H_{\mathrm{C}i}(s)I_i}{\left(1+U_iH_{\mathrm{pll}i}(s)\right)\left(sL_{\mathrm{f}}+H_{\mathrm{C}i}(s)\right)}\end{cases}$$

$$G_{\mathrm{APC}i}(s)=\begin{cases}H_{\mathrm{P}i}(s), & \textit{Constant Active Power Control}\\ \dfrac{H_{\mathrm{dc}i}(s)}{sU_{\mathrm{dc0}}C_{\mathrm{dc}}}, & \textit{Constant DC Voltage Control}\end{cases}$$

where Δ denotes the perturbed value of a variable; s is the Laplace operator; I_{ix} and I_{iy} are x-axis and y-axis components of the injected current at the point of interconnection of i^{th} CIG under the global reference xy-frames, respectively; U_{ix} and U_{iy} are x-axis and y-axis components of the terminal voltage at the point of interconnection of i^{th} CIG under the global reference xy-frames, respectively; $\boldsymbol{Y}_{\mathrm{CIG}i}(s)$ is the admittance model of the i^{th} CIG; when the i^{th} CIG adopts the constant active power control, $G_{\mathrm{APC}i}(s)= H_{\mathrm{P}i}(s)$; $H_{\mathrm{P}i}(s)$ is the transfer function of the constant active power control for i^{th} CIG; when the i^{th} CIG adopts the constant DC voltage control, $G_{\mathrm{APC}i}(s)=H_{\mathrm{dc}i}(s)/sC_{\mathrm{dc}}U_{\mathrm{dc0}}$; $H_{\mathrm{dc}i}(s)$ is the transfer function of the constant DC voltage control for the i^{th} CIG; C_{dc} is the DC capacitance; U_{dc0} is the terminal voltage of C_{dc}; $H_{\mathrm{pll}i}(s)$ is the transfer function of the PLL for the i^{th} CIG; $H_{\mathrm{C}i}(s)$ is the transfer function of the current control loop for i^{th} CIG; $f_{\mathrm{VF}}(s)$ is the voltage feedforward filter function in the current control loop; L_{f} is the filter inductance at the CIG side; I_i and U_i are the injected current and terminal voltage at the point of interconnection of the i^{th} CIG.

B. Network Modeling

The admittance model of the power network $\boldsymbol{Y}_{\mathrm{net}}(s)$ is [21]

$$\Delta\boldsymbol{I}_{xy}=\mathbf{Y}_{\mathrm{net}}(s)=\boldsymbol{B}\otimes\boldsymbol{F}(s)\Delta\boldsymbol{U}_{xy} \tag{3}$$

$$\boldsymbol{F}(s)=\frac{\omega_0}{\left(s^2+\omega_0^2\right)}\begin{bmatrix}s & \omega_0\\ -\omega_0 & s\end{bmatrix}$$

where $\Delta\boldsymbol{U}_{xy}=[\Delta U_{1x},\Delta U_{1y},\ldots,\Delta U_{nx},\Delta U_{ny}]^T$; $\Delta\boldsymbol{I}_{xy}=[\Delta I_{1x},\Delta I_{1y},\ldots,\Delta I_{nx},\Delta I_{ny}]^T$; $\boldsymbol{B}\in\boldsymbol{R}^{n\times n}$ represents the Thevenin equivalent admittance matrix only containing CIGs buses; $\otimes$ denotes Kronecker product; ω_0 is the rated angular frequency of ac grid.

C. MCIGS-AO Modeling

Combining (2) and (3), we have the modeling of the MCIGS-AO, and its characteristic equation can be represented by

$$\det\left\{\begin{bmatrix}\boldsymbol{Y}_{\mathrm{CIG1}}(s) & 0 & 0\\ 0 & \ddots & 0\\ 0 & 0 & \boldsymbol{Y}_{\mathrm{CIG}n}(s)\end{bmatrix}+\mathbf{Y}_{\mathrm{net}}(s)\right\}=0 \tag{4}$$

where det(·) denotes the determinant.

IV. Small-Signal Stability Analysis of the MCIGS-AO

Eq.(4) can be used to analyze the small-signal stability of the MCIGS-AO. However, this analysis is challenging due to the complex interaction between the converter control of many CIGs in the MCIGS-AO. Moreover, this analysis complexity is further increased when the CIG heterogeneity results from different actual operating conditions (i.e., injected current I_i and terminal voltage U_i of each CIG in (2)) coupled with different control parameters and configurations. To address the challenges, we first analyze multi-time scale converter control characteristics for CIGs to decouple the actual operating conditions from the converter control dynamics with a focus on the stability issues mainly caused by PLLs. Then, we transform the MCIGS-AO into a set of subsystems for the small-signal stability analysis.

A. Decoupling Actual CIG Operating Conditions from Converter Control Dynamics

By using the multi-time scale analysis for the converter control dynamics and assumption 1 in Section III, (2) can be rewritten as (5) when replacing I_i with $I_i= P_i/U_i$ in $Y_{\mathrm{g11}i}(s)$ and $Y_{\mathrm{g22}i}(s)$, i=1,…, n, where P_i is the actual active power output of the i^{th} CIG

$$\boldsymbol{Y}_{\mathrm{CIG}i}(s)=\begin{bmatrix} Y_{g11i}(s) & 0 \\ 0 & Y_{g22i}(s) \end{bmatrix} \tag{5}$$

$$\begin{cases} Y_{g11i}(s)\approx \dfrac{P_i H_{\mathrm{C}i}(s) G_{\mathrm{APC}i}(s)}{U_i\left[sL_{\mathrm{f}}+H_{\mathrm{C}i}(s)+U_i H_{\mathrm{C}i}(s) G_{\mathrm{APC}i}(s)\right]} \\ Y_{g22i}(s)\approx -\dfrac{P_i H_{\mathrm{pll}i}(s) H_{\mathrm{C}i}(s)}{U_i\left(1+U_i H_{\mathrm{pll}i}(s)\right)\left(sL_{\mathrm{f}}+H_{\mathrm{C}i}(s)\right)} \end{cases}$$

Remark: $\boldsymbol{Y}_{\mathrm{CIG}i}(s)$ in (5) is a simplified model for the one in (2). We will use $\boldsymbol{Y}_{\mathrm{CIG}i}(s)$ in (5) for analyzing the small-signal stability and proposing our method for fast identifying the small-signal stability issues in a MCIGS-AO. However, the full-order CIG model in (2) is used in Sections II, VI, and VII to verify the efficacy of the proposed method.

To decouple the actual operating conditions from the converter control dynamics, we can transfer the terminal voltage U_i and active power output P_i for each CIG from the CIG side to the network side. Thus, (4) can be rewritten as (6) by multiplying the numerator and denominator of $Y_{\mathrm{g}11i}(s)$ and $Y_{\mathrm{g}22i}(s)$ in $\boldsymbol{Y}_{\mathrm{CIG}i}(s)$ in (5) by U_i, i=1,…, n, and multiplying (4) by matrix $diag(U_i^2/P_i)$.

$$\det\left\{\begin{bmatrix} \hat{\boldsymbol{Y}}_{\mathrm{CIG}1}(s) & 0 & 0 \\ 0 & \ddots & 0 \\ 0 & 0 & \hat{\boldsymbol{Y}}_{\mathrm{CIG}n}(s) \end{bmatrix}+diag(\frac{U_i^2}{P_i})\boldsymbol{B}\otimes\boldsymbol{F}(s)\right\}=0 \tag{6}$$

$$\hat{\boldsymbol{Y}}_{\mathrm{CIG}i}(s)=\begin{bmatrix} \hat{Y}_{g11i}(s) & 0 \\ 0 & \hat{Y}_{g22i}(s) \end{bmatrix} \tag{7}$$

$$\begin{cases} \hat{Y}_{g11i}(s)\approx \dfrac{U_i H_{\mathrm{C}i}(s) G_{\mathrm{APC}i}(s)}{\left(sL_{\mathrm{f}}+H_{\mathrm{C}i}(s)\right)+U_i H_{\mathrm{C}i}(s) G_{\mathrm{APC}i}(s)} \\ \hat{Y}_{g22i}(s)\approx -\dfrac{U_i H_{\mathrm{pll}i}(s) H_{\mathrm{C}i}(s)}{\left(1+U_i H_{\mathrm{pll}i}(s)\right)\left(sL_{\mathrm{f}}+H_{\mathrm{C}i}(s)\right)} \end{cases}$$

where matrix $diag(U_i^2/P_i)$ is the diagonal matrix, in which the diagonal elements consist of U_i^2/P_i (i = 1 ...n).

In (6), it can be seen the converter control dynamics are decoupled from the actual operating conditions (i.e., terminal voltage U_i and active power output P_i for each CIG). Though there is still terminal voltage U_i at the CIG side, the voltage U_i coexists on the numerator and denominator of $\hat{Y}_{g11i}(s)$ and $\hat{Y}_{g22i}(s)$ in $\hat{\boldsymbol{Y}}_{\mathrm{CIG}i}(s)$, which will not lead to a significant change in the control dynamics of CIGs with voltage U_i.

B. Small-Signal Stability Analysis of MCIGS-AO

Based on (6) and (7), we will transform the MCIGS-AO into a set of simple subsystems to analyze the small-signal stability. To this end, we will first formulate an equivalent homogeneous MCIGS-AO that can characterize the small-signal stability of the original MCIGS-AO. That is, the dominant eigenvalues of the equivalent homogeneous MCIGS-AO can approximate those obtained from (6) for the original MCIGS-AO. Then, we decouple this equivalent homogeneous MCIGS-AO into a set of subsystems for the small-signal stability analysis.

According to the guidelines for renewable energy integrated into the power grid in different countries such as the US [18] and China [31], it is known that the terminal voltage U_i for each CIG changes in a range of 0.9~1.1p.u. for the system steady-state operating conditions. By including the differences in terminal voltages, control configurations, and control parameters for each CIG in (7), we formulate the equivalent homogeneous MCIGS-AO, where all equivalent CIGs have the same dynamics and are interconnected to the power network. More specifically, from (6), it can be observed that in the original MCIGS-AO, n heterogeneous converters modeled by $\hat{\boldsymbol{Y}}_{\mathrm{CIG}\,i}(s)$ (i=1,…,n) are connected to a weighted network characterized by $diag(U_i^2/P_i)\boldsymbol{B}$. To formulate the equivalent homogeneous MCIGS-AO interconnected through the same weighted network, (8) and (9) are defined to represent an equivalent converter in the equivalent homogeneous MCIGS-AO, where all n converters have the same $\boldsymbol{G}(s)$.

$$\boldsymbol{G}(s)=\sum\nolimits_{i=1}^{n} p_{1i}\hat{\boldsymbol{Y}}_{\mathrm{CIG}i}(s) \tag{8}$$

$$p_{1i}=u_{i1}v_{i1} \tag{9}$$

where $\boldsymbol{u}_1{}^T$and $\boldsymbol{v}_1$ are the left and right eigenvectors of the smallest eigenvalue of matrix $diag(U_i^2/P_i)\boldsymbol{B}$; u_{i1} and v_{i1} are the i^{th} elements of $\boldsymbol{u}_1{}^T$and $\boldsymbol{v}_1$, respectively; p_{1i} is the participation factor, which is normalized to satisfy $\sum_{i=1}^{n} p_{1i}=1$.

With (6)-(9), the characteristic equation of the equivalent homogeneous MCIGS-AO can be represented by

$$\det\left\{\begin{bmatrix} \boldsymbol{G}(s) & 0 & 0 \\ 0 & \ddots & 0 \\ 0 & 0 & \boldsymbol{G}(s) \end{bmatrix}+diag(\frac{U_i^2}{P_i})\boldsymbol{B}\otimes\boldsymbol{F}(s)\right\}=0$$

$$\Leftrightarrow \det\left\{\boldsymbol{I}_n\otimes\boldsymbol{\Lambda}(s)+diag(\frac{U_i^2}{P_i})\boldsymbol{B}\otimes\boldsymbol{I}_2\right\}=0 \tag{10}$$

$$\boldsymbol{\Lambda}(s)=\boldsymbol{G}(s)\boldsymbol{F}^{-1}(s) \tag{11}$$

where $\boldsymbol{I}_n$ is the n-dimensional identity matrix; $\boldsymbol{I}_2$ is the 2-dimensional identity matrix. Appendix B provides the proof that the equivalent homogeneous MCIGS-AO formulated based on (10) can characterize the small-signal stability of the original MCIGS-AO in (6).

Based on (10), we will further decompose this equivalent homogeneous MCIGS-AO into a set of single converter-interfaced generator subsystems (SCIGSs) for the small-signal stability analysis. Matrix $diag(U_i^2/P_i)\boldsymbol{B}$ is diagonalizable, and its eigenvalues are all positive according to the eigenvalues analysis in [21]. Thus, there exists a matrix $\boldsymbol{W}$ that can decompose matrix $diag(U_i^2/P_i)\boldsymbol{B}$ in (10) into a diagonal matrix, in which the diagonal elements consist of the eigenvalues (λ_i, i=1,…,n) in the order of $0\leq\lambda_1\leq,...,\leq\lambda_n$. That is,

$$\boldsymbol{W}^{-1}\left[diag(\frac{U_i^2}{P_i})\boldsymbol{B}\right]\boldsymbol{W}=diag\left(\lambda_i\right) \tag{12}$$

Combining (10) and (12) yields

$$\prod_{i=1}^{n}\det\left\{\boldsymbol{\Lambda}(s)+\lambda_i\boldsymbol{I}_2\right\}=0 \tag{13}$$

Eq.(13) shows that the equivalent homogeneous MCIGS-AO can be decoupled into n dynamically independent SCIGSs for the small-signal stability analysis. This equivalent

homogeneous MCIGS-AO is stable if and only if all the SCIGSs are stable. In other words, if one of the SCIGSs is unstable, the entire MCIGS-AO will be unstable. In all decoupled SCIGSs, CIGs are modeled by $\boldsymbol{G}(s)$ in $\boldsymbol{\Lambda}(s)$ to represent the same equivalent CIG dynamics. But they are connected to the grid by different equivalent line admittances, which are represented by different eigenvalues λ_i, i=1,…,n. For the given same equivalent CIGs dynamics (i.e., $\boldsymbol{\Lambda}(s)$), the stability of each SCIGS depends on the eigenvalues λ_i, i=1, …, n. The smaller eigenvalue λ_i means its corresponding SCIGS is more likely to be unstable. The smallest eigenvalue λ_1 corresponds to the SCIGS, which is the most critical. Thus, the small-signal stability of the equivalent homogeneous MCIGS-AO depends on the most critical subsystem as below.

$$\det\left\{\boldsymbol{\Lambda}(s)+\lambda_1\boldsymbol{I}_2\right\}=0 \tag{14}$$

Since the equivalent homogeneous MCIGS-AO can characterize the small-signal stability of the original heterogeneous MCIGS-AO, the stability of the original heterogeneous MCIGS-AO also depends on the most critical subsystem in (14). For the given $\boldsymbol{\Lambda}(s)$, the stability of the most critical subsystem depends on the smallest eigenvalue λ_1; thus, the small-signal stability of the original heterogeneous MCIGS-AO can be characterized by the smallest eigenvalue λ_1.

V. Proposed Method for Grid Strength Assessment under Actual Operating Conditions

Based on the analysis results in the previous section, we propose a method for assessing grid strength in terms of the small-signal stability to fast identify the small-signal stability issues and assess system stability margin in a MCIGS-AO.

A. The Proposed gOSCR and CgOSCR

According to the analysis results of Section IV. B, it is known that the small-signal stability of MCIGS-AO can be quantified based on the smallest eigenvalue λ_1 of matrix $diag(U_i^2/P_i)\boldsymbol{B}$. Thus, λ_1 depends on both the power network and actual operating conditions (e.g., active power output P_i and terminal voltage U_i for each CIG in the MCIGS-AO). Here, we define λ_1 as the generalized operational short-circuit ratio (gOSCR) to quantify grid strength of MCIGS-AO.

$$gOSCR=\min\lambda\left\{diag(\frac{U_i^2}{P_i})\boldsymbol{B}\right\} \tag{15}$$

where $\lambda\{\cdot\}$ denotes the eigenvalue calculation of a matrix.

To fast identify the small-signal instability issues via grid strength assessment, it needs to determine the threshold. The threshold is defined as the CgOSCR, which is the value of gOSCR that makes dominant eigenvalues of the system being just on the imaginary axis of the complex plane, indicating the system is critically stable under actual operating conditions. The CgOSCR can be analytically calculated based on (16) and (17). More specifically, according to our results of the small-signal stability analysis, it is known that the stability of the MCIGS-AO can be characterized by the most critical SCIGS in (14), showing that the original MCIGS-AO stability depends on λ_1 when the $\boldsymbol{\Lambda}(s)$ in (14) is given. Thus, for given $\boldsymbol{\Lambda}(s)$, there is a λ^*_1 that meets the dominant eigenvalue $s_c=j\omega_c$ of the system is just on the imaginary axis of the complex plane, indicating the system is critically stable. This λ^*_1 in (17) related to the critical stability is defined as CgOSCR, and thus gOSCR=CgOSCR can characterize the stability boundary of the MCIGS-AO.

$$\det\left(\boldsymbol{\Lambda}(s_c)+\lambda_1^*\cdot\boldsymbol{I}_2\right)=0 \tag{16}$$

$$\begin{cases}\mathrm{Re}\left(s_c\right)=0\\ CgOSCR=\lambda_1^*\end{cases} \tag{17}$$

where $\mathrm{Re}\{\cdot\}$ denotes the real part of a complex quantity.

The analytical expressions (16) and (17) provide the following benefits to CgOSCR. First, CgOSCR can be determined under actual operating conditions, even when the knowledge of the converter control structure and parameters are unknown (i.e., black-box model for CIGs). Specific algorithms are provided in Section VI. A and B. Second, (16) and (17) not only allow us to avoid a trial-and-error approach based on electromagnetic transient simulations to determine the CgOSCR, but they also enable us to explore insights into the impact on the system stability boundary due to various factors such as actual operating conditions, converter control parameters and configurations, and network structure.

B. The Proposed Method for Grid Strength Assessment

Based on the gOSCR and CgOSCR, we propose a method for fast identifying the small-signal stability issues and assessing system stability margin in a MCIGS-AO.

- To identify the system stability issues, we can compare the gOSCR with the CgOSCR: when gOSCR≥CgOSCR, the system small-signal stability is guaranteed; otherwise, the system becomes unstable.
- To assess the system margin, the following (18) is defined. In (18), the difference between the gOSCR and CgOSCR normalized by the CgOSCR reflects the relative degree to which system stability deviates from the stability boundary under actual operating conditions.

$$\beta\%\triangleq\frac{gOSCR-CgOSCR}{CgOSCR}\times100\% \tag{18}$$

The proposed β% addresses the shortcomings that the existing indices, such as SCR, ESCR, and gSCR as discussed in Section II, and their thresholds cannot assess system stability margin under actual operating conditions.

It should be noted that for the small-signal stability issues mainly caused by PLLs, the proposed method does not obtain a conservative result of system stability assessment. Furthermore, to deal with uncertain factors, grid planners and operators can use β% to assign a required system stability margin (e.g., β%=20%) to maintain system stability.

The proposed gOSCR and CgOSCR have the following features. First, gSCR and CgSCR [21] can be viewed as the special case of gOSCR and CgOSCR when a MCIGS-AO is operating under the rated operating condition (e.g., rated CIG capacity and rated terminal voltage). In other words, gOSCR and CgOSCR can be used for both rated and actual operating conditions. Second, the proposed gOSCR is the generalized version of the operational SCR (OSCR=U^2B/P), where P and U are the active power output and the terminal voltage of the CIG,

respectively; B is equivalent line admittance in the SCIGS [32]. Thus, OSCR and its threshold can be considered as the special case of gOSCR and CgOSCR when a MCIGS-AO is reduced to a SCIGS under actual operating conditions. Third, the proposed gOSCR and CgOSCR can also be used for assessing grid strength in terms of static voltage stability since the static voltage stability can be considered as a special case of small-signal stability at zero frequency band.

VI. Implementation of The Proposed Method

The implementation of the proposed method is illustrated in Fig. 4, and the major steps are summarized as follows.

Step 1) Calculate the gOSCR based on (15) by obtaining matrix $diag(U_i^2/P_i)\boldsymbol{B}$ according to the parameters of the power network, the active power output, and the terminal voltage of each CIG in the MCIGS-AO.

Step 2) Calculate the CgOSCR based on (16)-(17).

Step 3) Assess the small-signal stability and the normalized system stability margin β% based on gOSCR and CgOSCR.

Due to the intelligent property concern of vendors, the control structure and parameters of CIGs may be unknown. Since our proposed method is based on the admittance modeling, this allows us to measure the admittance of CIGs without needing the converter details. In the aforementioned Step 2), CgOSCR can be calculated when the knowledge of the converter control structure and parameters are either known or unknown (i.e., either the white-box model or black-box model for CIGs). In either of the two modeling scenarios, the CgOSCR calculation methods are detailed as follows.

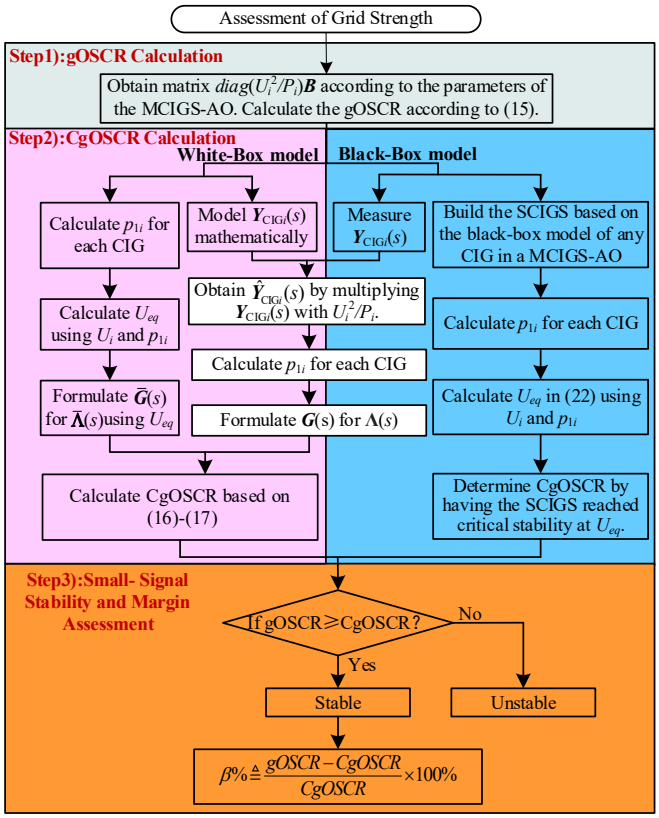

Fig. 4. Flowchart of the proposed method for small-signal stability assessment

and system stability margin assessment based on gOSCR and CgOSCR

A. CgOSCR Calculation Based on the White-Box model

When CIGs are modeled by the white-box model, the dynamic characteristics of CIGs are known in a MCIGS-AO. That is, $\boldsymbol{Y}_{CIGi}(s)$ in (5) for each CIG is known. Thus, the CgOSCR can be calculated by (Algorithm 1):

1. $\hat{\boldsymbol{Y}}_{CIGi}(s)$ in (7) is obtained for all CIGs by multiplying $\boldsymbol{Y}_{CIGi}(s)$ in (5) by U_i^2/P_i;
2. p_{1i} in (9) is calculated for each CIG by evaluating $\boldsymbol{u}_1{}^T$ and $\boldsymbol{v}_1$ about the smallest eigenvalue of matrix $diag(U_i^2/P_i)\boldsymbol{B}$;
3. $\boldsymbol{G}(s)$ in (8) is formulated for $\boldsymbol{\Lambda}(s)$ in (11) by $\hat{\boldsymbol{Y}}_{CIGi}(s)$ and p_{1i};
4. CgOSCR is calculated by $\boldsymbol{\Lambda}(s)$ and (16)-(17).

In this process, formulating the equivalent CIG model $\boldsymbol{G}(s)$ in (8) for the equivalent homogeneous system is important for calculating the CgOSCR based on the white-box model. However, it is challenging to formulate $\boldsymbol{G}(s)$ when the original MCIGS-AO has a large number of CIGs and each CIG has different operating conditions. $\boldsymbol{G}(s)$ in (8) is formulated by combining the dynamics of each CIG represented by $\hat{\boldsymbol{Y}}_{CIGi}(s)$ in (7). Each $\hat{\boldsymbol{Y}}_{CIGi}(s)$ is commonly a complex fraction expression with its terminal voltage for each CIG. For a MCIGS-AO with a large number of CIGs, when each CIG has different terminal voltages in $\hat{\boldsymbol{Y}}_{CIGi}(s)$, the resulting expression for $\boldsymbol{G}(s)$ will be high-order, which will thus increase the computational burden for calculating CgOSCR based on the white-box model. For example, in the three-converter system in Section VI.C, the denominator of $\boldsymbol{G}(s)$ is sixty-four-order ($\boldsymbol{G}(s)$ expression is presented in (43) of Appendix D). To address this challenge, we can replace $\boldsymbol{G}(s)$ with $\bar{\boldsymbol{G}}(s)$ by simplifying $\hat{\boldsymbol{Y}}_{CIGi}(s)$ as $\bar{\boldsymbol{Y}}_{CIGi}(s)$ in (19). When the small-signal stability issues are dominated by PLLs, $\hat{\boldsymbol{Y}}_{CIGi}(s)$ can be rewritten as $\bar{\boldsymbol{Y}}_{CIGi}(s)$ in (19). Thus, $\boldsymbol{G}(s)$ in (8) can be rewritten by $\bar{\boldsymbol{G}}(s)$ in (20) below, and also $\boldsymbol{\Lambda}(s)$ in (11) can be rewritten by $\bar{\boldsymbol{\Lambda}}(s)$ in (21) below. The derivation of $\bar{\boldsymbol{Y}}_{CIGi}(s)$ and $\bar{\boldsymbol{G}}(s)$ can be found in Appendix C.

$$\bar{\boldsymbol{Y}}_{CIGi}(s)=\begin{bmatrix}\dfrac{U_i G_{APC}(s)}{1+U_i G_{APC}(s)} & 0\\ 0 & -\dfrac{U_i H_{pll}(s)}{1+U_i H_{pll}(s)}\end{bmatrix} \tag{19}$$

$$\begin{aligned}\bar{\boldsymbol{G}}(s)&=\sum_{i=1}^{n} p_{1i}\bar{\boldsymbol{Y}}_{CIGi}(s)\\ &\approx\begin{bmatrix}\dfrac{U_{eq} G_{APC}(s)}{1+U_{eq} G_{APC}(s)} & 0\\ 0 & -\dfrac{U_{eq} H_{pll}(s)}{1+U_{eq} H_{pll}(s)}\end{bmatrix}\end{aligned} \tag{20}$$

$$\bar{\boldsymbol{\Lambda}}(s)=\bar{\boldsymbol{G}}(s)\boldsymbol{F}^{-1}(s) \tag{21}$$

$$\frac{1}{U_{eq}}=\sum_{i=1}^{n}\frac{p_{1i}}{U_i} \tag{22}$$

Compared with $\boldsymbol{G}(s)$ in (8), $\bar{\boldsymbol{G}}(s)$ in (20) models the combined dynamics of all CIGs by a simple expression with an equivalent voltage U_{eq} in (22), which combines all terminal voltages for all CIGs in a MCIGS-AO. For a MCIGS-AO with a large number of CIGs, this simple expression $\bar{\boldsymbol{G}}(s)$ in (20) can significantly reduce the computational burden to formulate $\boldsymbol{G}(s)$ for calculating CgOSCR by Algorithm 1. For example, in the three-converter system in Section VI.C, $\bar{\boldsymbol{G}}(s)$ in (44) of Appendix D is much simpler than $\boldsymbol{G}(s)$ in (43) of Appendix D. With the equivalent CIG model $\bar{\boldsymbol{G}}(s)$, CgOSCR can be calculated by (Algorithm 2):

1. p_{1i} in (9) is calculated for each CIG by evaluating $\boldsymbol{u}_1{}^T$ and $\boldsymbol{v}_1$ about the smallest eigenvalue of matrix $diag(U_i^2/P_i)\boldsymbol{B}$;
2. U_{eq} in (22) is evaluated using U_i and p_{1i};
3. $\bar{\boldsymbol{G}}(s)$ in (20) is formulated for $\bar{\boldsymbol{\Lambda}}(s)$ in (21) using converter control parameters and U_{eq};
4. CgOSCR is calculated by $\bar{\boldsymbol{\Lambda}}(s)$ and (16)-(17).

B. CgOSCR Calculation Based on the Black-Box model

When CIGs are modeled by the black-box model, their control parameters and configurations (e.g., $H_{Ci}(s)$, $H_{pll\,i}(s)$, $G_{APCi}(s)$ in (1)) are unknown in a MCIGS-AO. Since our proposed method is based on the admittance modeling, this allows us to measure the admittance $\boldsymbol{Y}_{CIGi}(s)$ of CIGs without needing the converter details to calculate the CgOSCR based on (16)-(17) following Algorithm 1.

In addition, we can calculate CgOSCR based on simulation or field tests as well. To this end, a SCIGS that represents the most critical subsystem in (16) can be formulated in a simulation platform to determine the CgOSCR. This SCIGS consists of a single CIG connected to the grid via the equivalent line susceptance OSCR, which is a function of CIG terminal voltage U, CIG power output P, and line susceptance B. The characteristic equation of the most critical subsystem is:

$$\det\left(\hat{\boldsymbol{Y}}_{\mathrm{b}}(s)\boldsymbol{F}^{-1}(s)+OSCR(U,P,B)\cdot\boldsymbol{I}_2\right)=0 \tag{23}$$

where $\hat{\boldsymbol{Y}}_{\mathrm{b}}(s)$ is the admittance model of the black-box model of CIGs; OSCR=U^2B/P.

In the SCIGS, the CgOSCR can be calculated by the following steps (Algorithm 3): first, we build the most critical subsystem using equivalent line susceptance, voltage source, and the black-box model of CIGs in a MCIGS-AO using the hardware-in-the-loop simulation platform or digital simulation platform. The characteristic equation of the most critical subsystem is shown in (23); then, p_{1i} in (9) is calculated for each CIG by evaluating $\boldsymbol{u}_1{}^T$ and $\boldsymbol{v}_1$ about the smallest eigenvalue of matrix $diag(U_i^2/P_i)\boldsymbol{B}$; next, U_{eq} in (22) is calculated using U_i and p_{1i}; and finally, the CgOSCR is determined by changing the line inductance and source voltage while keeping $U = U_{\mathrm{eq}}$ constant in the created subsystem to find $OSCR^*$ in (24), which meets the dominant eigenvalue $s_{\mathrm{c1}}=j\omega_{\mathrm{c1}}$ of the most critical subsystem is just on the imaginary axis of the complex plane. This $OSCR^*$is the CgOSCR.

$$\begin{cases}\det\left(\hat{\boldsymbol{Y}}_{\mathrm{b}}(s_{c1})\boldsymbol{F}^{-1}(s_{c1})+OSCR^*\cdot\boldsymbol{I}_2\right)=0\\ \mathrm{Re}\left(s_{c1}\right)=0\\ CgOSCR=OSCR^*=\dfrac{U_{eq}^2}{P}B^*\end{cases} \tag{24}$$

C. Illustrative Case

To illustrate the proposed method as shown in Fig. 4, let us consider the three-converter system described in Section II. By following the procedure in Fig. 4, the gOSCR and CgOSCR can be calculated in this system for stability identification.

In step 1), we evaluate gOSCR based on (15) after calculating matrix $diag(U_i^2/P_i)\boldsymbol{B}$. The admittance matrix $\boldsymbol{B}$ in (25) and matrix $diag(U_i^2/P_i)$ in (26) can be calculated according to the network topology and parameters of the three-converter system given in TABLE A. I of Appendix A and the terminal voltages and active power outputs of three CIGs in TABLE I. Thus, the gOSCR can be obtained in (27).

$$\boldsymbol{B}=\begin{bmatrix}41.51 & -1.89 & -1.89\\ -1.89 & 11.32 & -1.89\\ -1.89 & -1.89 & 4.31\end{bmatrix} \tag{25}$$

$$diag\left(\frac{U_i^2}{P_i}\right)=\begin{bmatrix}4.51 & & \\ & 1.06 & \\ & & 0.81\end{bmatrix} \tag{26}$$

$$\begin{aligned}gOSCR&=\min\lambda\left\{diag\left(\frac{U_i^2}{P_i}\right)\boldsymbol{B}\right\}\\ &=\min\lambda\left\{\begin{bmatrix}187.31 & -2.13 & -1.70\\ -7.98 & 11.98 & -1.60\\ -7.64 & -1.91 & 3.49\end{bmatrix}\right\}=3.04\end{aligned} \tag{27}$$

In step 2), when CIGs are modeled by the white-box model, we evaluate CgOSCR using (16)-(17) and $\bar{\boldsymbol{\Lambda}}(s)$. First, p_{1i} in (9) is calculated for each CIG by evaluating $\boldsymbol{u}_1{}^T$ and $\boldsymbol{v}_1$ about the smallest eigenvalue of matrix $diag(U_i^2/P_i)\boldsymbol{B}$. The results are p_{11}=0.01, p_{12}=0.06, and p_{13}=0.93. Then, U_{eq} in (28) is calculated using terminal voltages U_i for each CIG as shown in TABLE I and the evaluated p_{1i}. Next, $\bar{\boldsymbol{\Lambda}}(s)$ in (31) can be obtained by $\bar{\boldsymbol{G}}(s)$ in (29) and $\boldsymbol{F}(s)$ in (30), where $\bar{\boldsymbol{G}}(s)$ in (29) is obtained by U_{eq} in (28) and the converter control configurations and parameters presented in TABLE A. I of Appendix A. The detailed representation of $\bar{\boldsymbol{\Lambda}}(s)$ is presented in (45) of Appendix D due to its complexity. Finally, the CgOSCR can be determined based on (16)-(17) and $\bar{\boldsymbol{\Lambda}}(s)$. According to the analysis in Section V.A, (16) can be viewed as an equivalent CIG is connected to the grid via the equivalent line susceptance, which is the smallest eigenvalue λ_1 of matrix $\mathrm{diag}(U_i^2/P_i)\boldsymbol{B}$ and thus is a function of CIG terminal voltage U_i, CIG power output P_i, and network structure $\boldsymbol{B}$. In the equivalent subsystem, we will change the equivalent line susceptance with given U_{eq} to find λ^*_1, which meets that dominant eigenvalue $s_{\mathrm{c}}=j\omega_{\mathrm{c}}$ of the most critical subsystem is just on the imaginary

axis of the complex plane. The corresponding λ^*_1 is the CgOSCR. Thus, we have s_c=-0.008+j80.4 ≈ j80.4 and CgOSCR=3.55.

$$\frac{1}{U_{eq}}=\sum_{i=1}^{n}\frac{p_{1i}}{U_i}=1.1\Leftrightarrow U_{eq}=0.90 \tag{28}$$

$$\bar{\boldsymbol{G}}(s)=\begin{bmatrix}\dfrac{0.9s^2+7.2s}{0.038s^3+0.9s^2+7.2s} & 0\\ 0 & \dfrac{-4.05s^3-6480s^2}{s^4+4.05s^3+6480s^2}\end{bmatrix} \tag{29}$$

$$\boldsymbol{F}(s)=\begin{bmatrix}\dfrac{314.2\ \mathrm{s}}{s^2+9.87e04} & \dfrac{9.87e04}{s^2+9.87e04}\\ \dfrac{-9.87e04}{s^2+9.87e04} & \dfrac{314.2\ \mathrm{s}}{s^2+9.87e04}\end{bmatrix} \tag{30}$$

$$\bar{\boldsymbol{\Lambda}}(s)=\bar{\boldsymbol{G}}(s)\boldsymbol{F}^{-1}(s) \tag{31}$$

In step 2), when CIGs are modeled by the black-box model, the CgOSCR can be calculated following Algorithms 1 or 3. Since the specific steps for Algorithm 1 are similar to those in the white-box model above, except admittance $\boldsymbol{Y}_{\mathrm{CIG}i}(s)$ of CIGs need to be measured, here we specify Algorithm 3: first, we can create the most critical subsystem using equivalent line susceptance, voltage source, and the black-box model of CIGs in a MCIGS-AO using a hardware-in-the-loop simulation platform or digital simulation platform; then, the CgOSCR can be determined by changing the line inductance and source voltage while keeping U=U_{eq}=0.9 constant in the created subsystem to find *OSCR** in (24), which makes the dominant eigenvalues of the subsystem being just on the imaginary axis. *OSCR**=3.55 can be obtained, and thus CgOSCR=3.55, which is equal to the one analytically calculated.

In step 3), the system stability can be identified by comparing gOSCR with CgOSCR. The identification result is presented in TABLE III. It can be seen from TABLE III that gOSCR= 3.04 is smaller than CgOSCR= 3.55. This suggests that the system under the actual operating conditions is unstable following the disturbance, which is consistent with the observation from the electromagnetic transient simulation results in Fig. 2.

By comparing the results of TABLE III with those of TABLE II and Fig. 2, it shows that the proposed method can address the concern of the existing methods to identify the small-signal stability issues in a MCIGS-AO. In the next section, we will validate the proposed method in different power systems with high CIG penetration.

TABLE III
EVALUATION RESULTS OF gOSCR AND CgOSCR UNDER THE ACTUAL OPERATING CONDITIONS PRESENTED IN TABLE I

gOSCR	CgOSCR	Stability		β%
3.04	3.55	3.04<3.55	Unstable	N/A

VII. SIMULATION RESULTS

In this section, we will validate the effectiveness of the proposed method on a modified IEEE 39-bus system and a practical power system (i.e., Hami wind power system in China) by modal analysis and electromagnetic transient simulation. A conditional simulation result on the modified IEEE 39-bus system is given to compare the proposed method with those well-known SCR methods. It should be noted that while our method is proposed based on the simplified CIG model shown in (5), the full-order modeling for all CIGs without any approximations is used in these two systems to verify the efficacy of the proposed method.

A. Case Studies on the Modified IEEE 39-Bus System

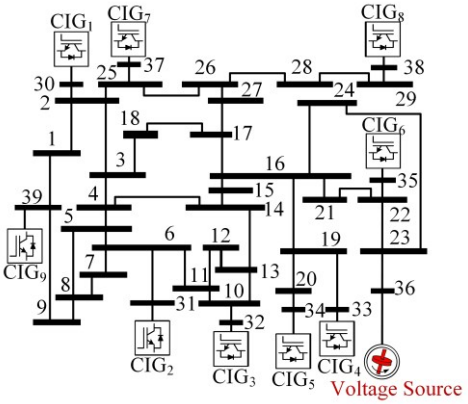

Fig. 5. One-line diagram of IEEE 39-bus system.

In the IEEE 39-bus system as shown in Fig. 5, nine CIGs are placed at nodes 30~35, 37~39. The control parameters of these nine CIGs and the parameters of the power network in the system are shown in TABLE E. I of Appendix E. This system has been created on MATLAB/Simulink.

TABLE IV
EVALUATION RESULTS OF gOSCR AND CgOSCR UNDER DIFFERENT SCENARIOS OF ACTUAL OPERATING CONDITIONS

Scenario	U/p.u. P/p.u.	gOSCR	CgOSCR	Stability	β%
a	The detailed operating	4.28	4.41	unstable	N/A
b	conditions for nine CIGs	4.42	4.40	stable	0.5%
c	are given in TABLE E. II of Appendix E	11.20	4.61	stable	143%

To verify the efficacy of the proposed method, three scenarios of actual operating conditions are considered for the system, and they are shown in TABLE IV. Under these three scenarios of actual operating conditions, gOSCR and CgOSCR are evaluated, and their evaluation results are also presented in TABLE IV. In addition, modal analysis and electromagnetic transient simulation are performed in the system under these three scenarios, and their results are shown in Fig. 6 and Fig. 7. In the electromagnetic transient simulation, a disturbance is applied to the infinite bus in the system at 0.20s to cause the voltage to rise by 5% and then is cleared at 0.25s. This same disturbance is applied to the system under these three scenarios.

The efficacy of the proposed method is validated by comparing the results of the proposed method in TABLE IV with those of modal analysis and electromagnetic transient simulation in Fig. 6 and Fig. 7. It can be observed from TABLE IV that the proposed method identifies the system is unstable under scenario a), but the system is stable under the other two scenarios. The observation results are consistent with the results of modal analysis, as shown in Fig. 6. In Fig 6, the dominant eigenvalues of the system under scenario a) are located on the right-hand of the complex plane, which indicates an unstable system; on the other hand, the dominant eigenvalues of the system under the other two scenarios are located on the left-hand of the complex plane, which indicates the stable system.

Also, the observation results from TABLE IV are consistent with the results of the electromagnetic transient simulation, as shown in Fig. 7. In Fig 7, there are divergent voltage oscillations when the system under scenario a) follows a disturbance; but such voltage oscillations do not occur in the system when the system under the other two scenarios follows the same disturbance. Thus, this consistency between the results of the proposed method and those of modal analysis and electromagnetic transient simulation verifies the effectiveness of the proposed method in the IEEE 39-bus system.

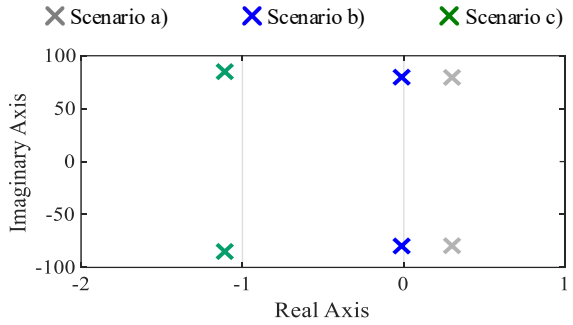

Fig. 6. Dominant eigenvalues of the IEEE 39-bus system under different scenarios of actual operating conditions

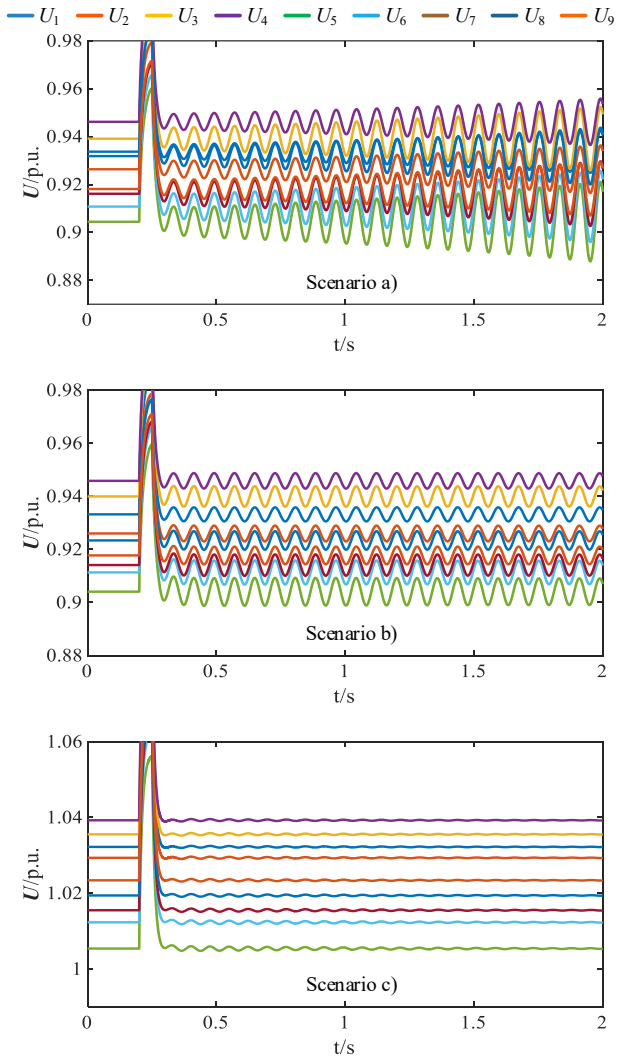

Fig. 7. Trajectories of terminal voltages of CIGs in the IEEE 39-bus system under different scenarios of actual operating conditions

In addition, the proposed gOSCR-based method is compared with the existing methods for grid strength assessment in the system under scenario a) of operating conditions in TABLE IV. Without the loss of generality, we still select those three typical indices in TABLE II for this illustration. The comparison results are presented in TABLE V, where the thresholds of those existing indices are selected according to [13] [18], and the threshold for gSCR is calculated based on the method in [21].

It can be seen from TABLE V that the evaluation results of SCR[12], ESCR[17], and gSCR [21] are larger than their individual thresholds. This suggests that there are no small-signal stability issues in the system under scenario a) of operating conditions in TABLE IV. The identification results are contrary to the observation from the modal analysis results in Fig. 6 and electromagnetic transient simulation results in Fig. 7. On the other hand, the evaluation results of the gOSCR are consistent with those from modal analysis and electromagnetic transient simulation. Thus, the proposed method is effective in identifying the small-signal stability issues under scenario a), while these existing techniques provide misleading results to identify the small-signal stability issues.

TABLE V
EVALUATION RESULTS OF SCR, ESCR, gSCR, gOSCR, AND THEIR THRESHOLDS UNDER THE OPERATING CONDITION SCENARIO A) OF TABLE IV

Indices	gOSCR	SCR	ESCR	gSCR[21]
Values	4.28	8.44	3.83	4.60
Thresholds	4.41	3[13]	3[18]	4.30
System Stability Identification	4.28 <4.41	8.44>3	3.83>3	4.60>4.30
	Unstable	Stable	Stable	Stable
	Consistent with the identification results from the simulation	Contrary to the identification results obtained from the modal analysis and electromagnetic transient simulation		

B. Case Studies on a Practical Power System

The efficacy of the proposed method is further verified in a practical power system with high wind penetration in China (i.e., Hami wind power system in China) via electromagnetic transient simulation. As shown in Fig. 8, the system is divided into five regions marked as ①, ②, ③, ④, and ⑤, respectively. The system has 31 wind energy plants and 54 equivalent CIGs, where the control parameters of CIGs in regions ① and ② are different from the control parameters of CIGs in regions ③, ④ , and ⑤, which are given in TABLE E. III of Appendix E. The parameters of the system network topology are given in TABLE E. III of Appendix E as well. In the system, three scenarios of actual operating conditions are considered, and they are shown in TABLE VI, where the actual operating conditions for 54 CIGs are different from each other. The corresponding gOSCR and CgOSCR are evaluated, and they are gOSCR=1.72, 2.25, 1.82 and CgOSCR=1.85, 1.90, 1.82, which are also presented in TABLE VI. Under the three scenarios of actual operating conditions, electromagnetic transient simulations are performed in the system following the same disturbance, which is applied to the infinite bus (i.e., bus 93) in the system at 0.10s to cause the voltage to drop by 5%. Fig. 9 below shows the power trajectories of all converter terminal buses in the system

following the disturbance when different scenarios of actual operating conditions are considered. Fig. 10 shows the three-phase voltage trajectories at bus 1 in the system following the disturbance when each scenario is considered.

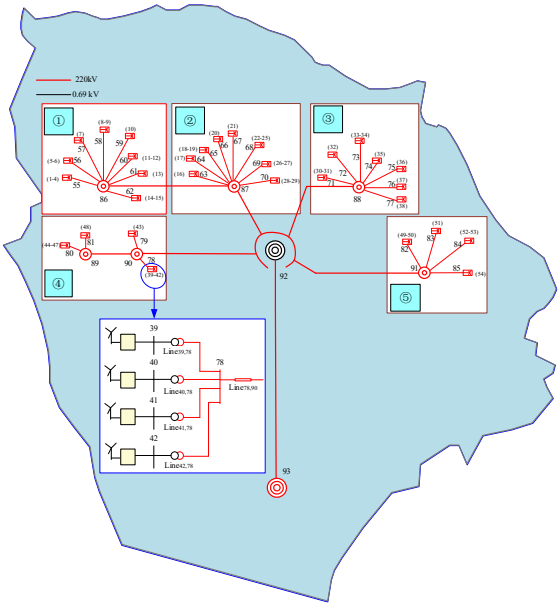

Fig. 8. Network topology of Hami wind power system in China.

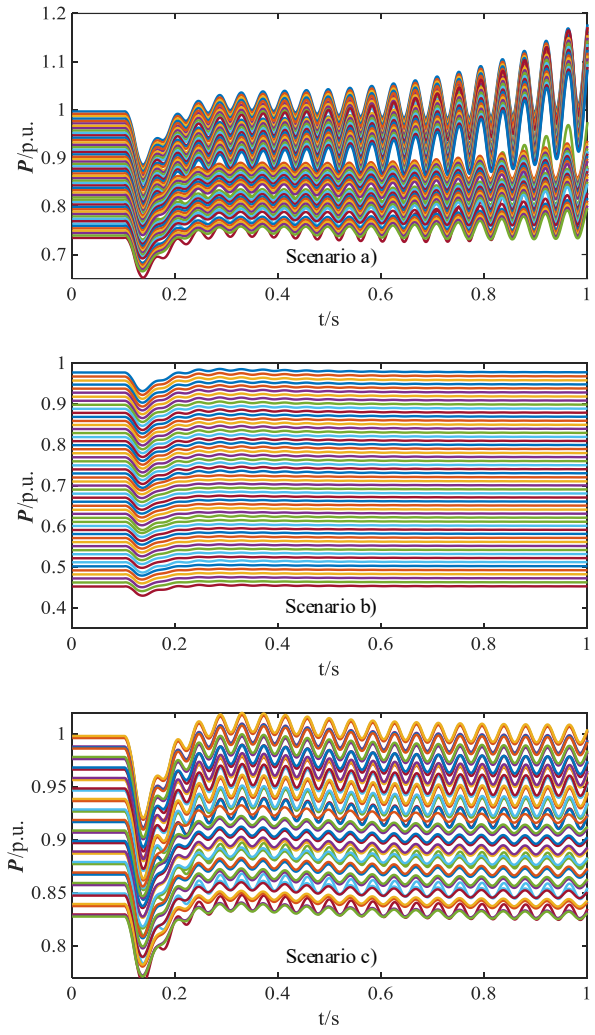

Fig. 9. Trajectories of CIG active power outputs in the Hami wind power system under different scenarios of actual operating conditions

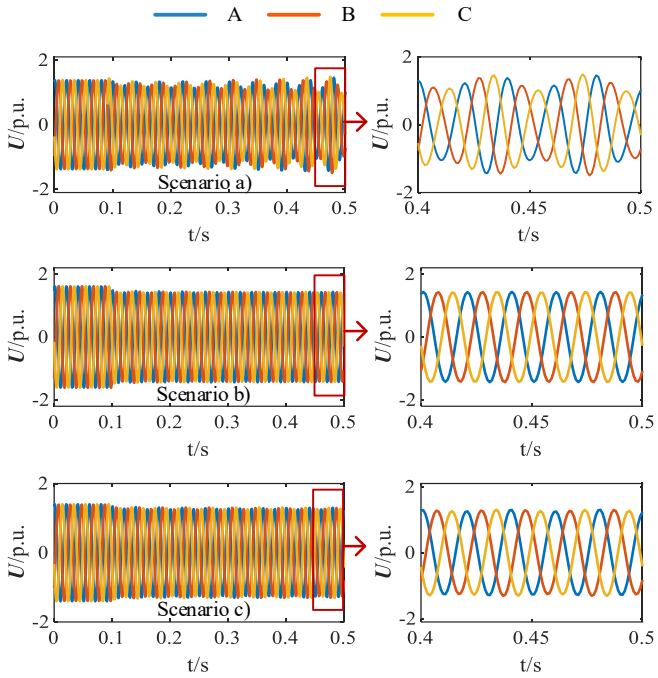

Fig. 10. Trajectories of three-phase voltage at bus 1 in the Hami wind power system under different scenarios of actual operating conditions (A, B, and C represent A, B, and C phase voltages, respectively)

TABLE VI
EVALUATION RESULTS OF gOSCR AND CgOSCR IN HAMI WIND POWER SYSTEM UNDER DIFFERENT SCENARIOS OF ACTUAL OPERATING CONDITIONS

Scenario	*U*/pu	*P*/pu	gOSCR	CgOSCR	Stability	*β*%
a	The detailed operating		1.72	1.85	unstable	N/A
b	conditions for 54 CIGs		2.25	1.90	stable	18.4%
c	are given in TABLE E. IV of Appendix E		1.82	1.82	critically stable	0

The efficacy of the proposed method is validated in the practical system since the identification results based on the proposed method are consistent with those based on electromagnetic transient simulation. The identification results of the proposed method are presented in TABLE VI. It can be observed from TABLE VI, Fig. 9 and Fig. 10 that when gOSCR=1.72<CgOSCR=1.85, indicating the unstable system under actual operating condition scenario a), Fig. 9 and Fig. 10 show divergent power oscillations and divergent three-phase voltage oscillations; when gOSCR=2.25>CgOSCR=1.90, suggesting the stable system under scenario b), Fig. 9 and Fig. 10 show the converged power oscillations and converged three-phase voltage oscillations; and when gOSCR=1.82= CgOSCR=1.82, meaning the critically stable system under scenario c), Fig. 9 and Fig. 10 show approximate undamped power oscillations and approximate undamped three-phase voltage oscillations. Thus, this consistency between the identification results of the proposed method and those from electromagnetic simulation verifies the effectiveness of the proposed method in the practical large-scale power system with high wind penetration.

VIII. CONCLUSION

In this paper, a method was proposed for grid strength assessment to fast identify the small-signal stability issues

mainly caused by PLLs in a MCIGS-AO. The method is applicable for a practical power system with high CIG penetration, even when converter details are unknown. The proposed method addressed the shortcomings of the existing techniques that they were developed based on the rated operating conditions and thus provided misleading identification results of the small-signal stability in a MCIGS-AO. The existing gSCR-based approach is a special case of the method proposed in this paper when a MCIGS-AO is operating under the rated operating conditions. In our future research, the proposed method will be extended to the stability analysis of a MCIGS-AO under large disturbance conditions.

APPENDIX A

TABLE A. I
PARAMETERS OF THE THREE-CONVERTER SYSTEM (PER-UNIT)

Parameters of the PLL-Based Control					
PI parameters of the current control loop: 0.3, 10					
PI parameters of the dc voltage control loop: 0.5, 8					
PI parameters of the PLL: 4.5, 7200					
Parameters of the voltage feedforward filter: 0.001					
Filter inductance: 0.05,					
DC capacitance and base voltage of dc bus: 0.038, 1					
Rated capacity of converters: 1					
Parameters of Power Network in the Three-Converter System					
Line $_{12}$	0.53	Line $_{23}$	0.53	Line $_{13}$	0.53
Line $_{14}$	0.027	Line $_{24}$	0.133	Line $_{34}$	1.86

APPENDIX B

Detailed Proof of Equation (10) Approximating (6)

Proposition III.1 below proves that the equivalent homogeneous MCIGS-AO based on (10) can characterize the small-signal stability of the original heterogeneous MCIGS-AO in (6).

Proposition III.1 Let $\lambda_j(s)$ and $\bar{\lambda}_j(s)$ $(j=1,2)$ be the dominant eigenvalue function of the original heterogeneous MCIGS-AO and its equivalent homogeneous MCIGS-AO, respectively, and they are pertinent to the two systems' dominant eigenvalues. Then, the loci of $\lambda_j(s)$ and $\bar{\lambda}_j(s)$ have the following relationship:

$$\lambda_j(s)=\bar{\lambda}_j(s)+\boldsymbol{O}\left(\left\|\boldsymbol{Y}_{\text{het}}(s)-\bar{\boldsymbol{Y}}_{\text{hom}}(s)\right\|\right)\ j=1,2 \tag{32}$$

where

$$\begin{cases}\boldsymbol{Y}_{\text{het}}(s)=\begin{bmatrix}\hat{\boldsymbol{Y}}_{\text{CIG1}}(s)\boldsymbol{F}^{-1}(s) & 0 & 0\\ 0 & \ddots & 0\\ 0 & 0 & \hat{\boldsymbol{Y}}_{\text{CIG}n}(s)\boldsymbol{F}^{-1}(s)\end{bmatrix}+diag(\frac{U_i^2}{P_i})\boldsymbol{B}\otimes\boldsymbol{I}_2\\ \bar{\boldsymbol{Y}}_{\text{hom}}(s)=\begin{bmatrix}\boldsymbol{G}(s)\boldsymbol{F}^{-1}(s) & 0 & 0\\ 0 & \ddots & 0\\ 0 & 0 & \boldsymbol{G}(s)\boldsymbol{F}^{-1}(s)\end{bmatrix}+diag(\frac{U_i^2}{P_i})\boldsymbol{B}\otimes\boldsymbol{I}_2\end{cases}$$

where $\boldsymbol{O}(\cdot)$ denotes the second-order and much higher-order approximate error of a function; $\|\cdot\|$ denotes the norm of any matrix.

Proof: Based on the small-signal stability analysis of the equivalent homogeneous system in Section IV.B, it is known that $\bar{\lambda}_j(s)$ can be obtained from the most critical subsystem decoupled from the equivalent homogeneous system. Thus, $\bar{\lambda}_j(s)$ can be formulated:

$$\begin{aligned}\bar{\lambda}_j(s)&=\left(\boldsymbol{u}_1^T\otimes\boldsymbol{\psi}_j^T(s)\right)\bar{\boldsymbol{Y}}_{\text{hom}}(s)\left(\boldsymbol{v}_1\otimes\boldsymbol{\tau}_j(s)\right)\\&=\alpha_j(s)+\lambda_1\quad(j=1,2)\end{aligned} \tag{33}$$

where $\boldsymbol{\psi}(s)=\left[\boldsymbol{\psi}_1(s)\ \ \boldsymbol{\psi}_2(s)\right]$ and $\boldsymbol{\tau}(s)=\left[\boldsymbol{\tau}_1(s)\ \ \boldsymbol{\tau}_2(s)\right]$; $\boldsymbol{\psi}_j^T(s)$ and $\boldsymbol{\tau}_j(s)$ $(j=1,2)$ represent the normalized left and right eigenvectors of $\boldsymbol{G}(s)\boldsymbol{F}^{-1}(s)$ corresponding to the characteristic function $\alpha_j(s)(j=1,2)$, and they satisfy $\boldsymbol{\psi}_j^T(s)\boldsymbol{\tau}_j(s)=1,\ (j=1,2)$.

In the original heterogeneous MCIGS-AO, $\boldsymbol{Y}_{\text{het}}(s)$ can be considered as a result of imposing a perturbation on $\bar{\boldsymbol{Y}}_{\text{hom}}(s)$. According to Theorem 2.3 in [33], the dominant eigenvalue function $\lambda_j(s)$ $(j=1,2)$ for $\boldsymbol{Y}_{\text{het}}(s)$ can be represented as:

$$\begin{aligned}\lambda_j(s)&=\left(\boldsymbol{u}_1^T\otimes\boldsymbol{\psi}_j^T(s)\right)\boldsymbol{Y}_{\text{het}}(s)\left(\boldsymbol{v}_1\otimes\boldsymbol{\tau}_j(s)\right)+\boldsymbol{O}\left(\left\|\boldsymbol{Y}_{\text{het}}(s)-\bar{\boldsymbol{Y}}_{\text{hom}}(s)\right\|\right)\\&=\boldsymbol{\psi}_j^T(s)\left[\sum\nolimits_{i=1}^{n}u_{i1}v_{i1}\cdot\hat{\boldsymbol{Y}}_{\text{CIG}i}(s)\cdot\boldsymbol{F}^{-1}(s)\right]\boldsymbol{\tau}_j(s)+\lambda_1\\&\quad+\boldsymbol{O}\left(\left\|\boldsymbol{Y}_{\text{het}}(s)-\bar{\boldsymbol{Y}}_{\text{hom}}(s)\right\|\right)\\&=\boldsymbol{\psi}_j^T(s)\boldsymbol{G}(s)\boldsymbol{F}^{-1}(s)\boldsymbol{\tau}_j(s)+\lambda_1+\boldsymbol{O}\left(\left\|\boldsymbol{Y}_{\text{het}}(s)-\bar{\boldsymbol{Y}}_{\text{hom}}(s)\right\|\right)\\&=\bar{\lambda}_j(s)+\boldsymbol{O}\left(\left\|\boldsymbol{Y}_{\text{het}}(s)-\bar{\boldsymbol{Y}}_{\text{hom}}(s)\right\|\right)\quad(j=1,2)\end{aligned} \tag{34}$$

This *completes* the proof ■.

APPENDIX C

Detailed Proof of Equation (19)-(22)

Since most of the small-signal stability issues are dominated by PLLs, and the response speed of PLLs is much lower than the current control loop[6]-[9], the fast dynamics of the current control loop can be ignored to focus on the stability issues mainly caused by PLLs in the MCIGS-AO according to approximation 2. $\hat{\boldsymbol{Y}}_{\text{CIG}i}(s)$ can be simplified as:

$$\bar{\boldsymbol{Y}}_{\text{CIG}i}(s)=\begin{bmatrix}\dfrac{U_iG_{\text{APC}}(s)}{1+U_iG_{\text{APC}}(s)} & 0\\ 0 & -\dfrac{U_iH_{\text{pll}}(s)}{1+U_iH_{\text{pll}}(s)}\end{bmatrix} \tag{35}$$

where $\bar{\boldsymbol{Y}}_{\text{CIG}i}(s)$ is the simplified model of $\hat{\boldsymbol{Y}}_{\text{CIG}i}(s)$.

Since the converter itself is stable, we can obtain the impedance model $\bar{\boldsymbol{Z}}_{\text{CIG}i}(s)$ below by inversing $\bar{\boldsymbol{Y}}_{\text{CIG}i}(s)$ in (35).

$$\bar{\boldsymbol{Z}}_{\text{CIG}i}(s)=\begin{bmatrix}1+\dfrac{1}{U_iG_{\text{APC}}(s)} & 0\\ 0 & -1-\dfrac{1}{U_iH_{\text{pll}}(s)}\end{bmatrix} \tag{36}$$

Combining (36) and inversing the equivalent admittance model of the power network in (6), we can obtain the

characteristic equation of the MCIGS-AO based on the impedance model.

$$\det\left\{\begin{bmatrix}\bar{\boldsymbol{Z}}_{\mathrm{CIG1}}(s) & 0 & 0\\ 0 & \ddots & 0\\ 0 & 0 & \bar{\boldsymbol{Z}}_{\mathrm{CIGn}}(s)\end{bmatrix}+\boldsymbol{B}^{-1}diag(\frac{P_i}{U_i^2})\otimes\boldsymbol{F}^{-1}(s)\right\}=0 \quad (37)$$

According to the analysis results in Section IV.B, we also can formulate the equivalent homogeneous MCIGS-AO, where all equivalent CIGs are modeled by $\boldsymbol{Z}(s)$ below.

$$\boldsymbol{Z}(s)=\sum_{i=1}^{n}p_{1i}\bar{\boldsymbol{Z}}_{\mathrm{CIG}i}(s) \quad (38)$$

$$p_{1i}=u_{i1}v_{i1} \quad (39)$$

$$\boldsymbol{Z}(s)=\begin{bmatrix}1+\dfrac{1}{U_{eq}G_{\mathrm{APC}}(s)} & 0\\ 0 & -1-\dfrac{1}{U_{eq}H_{\mathrm{pll}}(s)}\end{bmatrix} \quad (40)$$

$$\frac{1}{U_{eq}}=\sum_{i=1}^{n}\frac{p_{1i}}{U_i} \quad (41)$$

where $\boldsymbol{u}_1{}^T$and $\boldsymbol{v}_1$ are the left and right eigenvectors about the smallest eigenvalue of matrix $diag(U_i^2/P_i)\boldsymbol{B}$ while $\boldsymbol{u}_1{}^T$and $\boldsymbol{v}_1$ are also the left and right eigenvectors about the largest eigenvalue of matrix $\boldsymbol{B}^{-1}diag(P_i/U_i^2)$ since if $(\lambda,\boldsymbol{u})$ is the eigenpairs of the matrix, $(\lambda^{-1},\boldsymbol{u})$ is the eigenpairs of its inverse matrix [34].

The equivalent CIG model $\boldsymbol{G}(s)$ can be approximated by $\bar{\boldsymbol{G}}(s)$ below by inversing $\boldsymbol{Z}(s)$ in (40):

$$\bar{\boldsymbol{G}}(s)=\begin{bmatrix}\dfrac{U_{eq}G_{\mathrm{APC}}(s)}{1+U_{eq}G_{\mathrm{APC}}(s)} & 0\\ 0 & -\dfrac{U_{eq}H_{\mathrm{pll}}(s)}{1+U_{eq}H_{\mathrm{pll}}(s)}\end{bmatrix} \quad (42)$$

$$\bar{\boldsymbol{\Lambda}}(s)=\bar{\boldsymbol{G}}(s)\boldsymbol{F}^{-1}(s)$$

$$=\begin{bmatrix}\dfrac{0.9s^5+7.2s^4+8.883e04s^3+7.106e05s^2+1.71e-26s}{11.94s^5+282.7s^4+1.181e06s^3+2.791e07s^2+2.232e08s} & \dfrac{-282.7s^4-2262s^3-2.791e07s^2-2.232e08s}{11.94s^5+282.7s^4+1.181e06s^3+2.791e07s^2+2.232e08s}\\ \dfrac{-1272s^5-2.036e06s^4-1.256e08s^3-2.009e11s^2}{314.2s^6+1272s^5+3.304e07s^4+1.256e08s^3+2.009e11s^2} & \dfrac{-4.05s^6-6480s^5-3.997e05s^4-6.396e08s^3+1.026e-22s^2}{314.2s^6+1272s^5+3.304e07s^4+1.256e08s^3+2.009e11s^2}\end{bmatrix} \quad (45)$$

APPENDIX E

TABLE E. I
PARAMETERS OF THE IEEE 39-BUS SYSTEM (PER-UNIT)

Parameters of the PLL-Based Control					
PI parameters of the current control loop: 0.3, 10					
PI parameters of the dc voltage control loop: 0.5, 8					
PI parameters of the PLL: 4, 7200					
Parameters of the voltage feedforward filter: 0.001					
Filter inductance: 0.05,					
DC capacitance and base voltage of dc bus: 0.038, 1					
Rated capacity of converters: 1					
Parameters of Power Network in the IEEE 39-Bus System					
Line 1,2	0.0058	Line 1,39	0.0140	Line 2,3	0.0021
Line 2,30	0.0980	Line 3,4	0.0030	Line 3,18	0.0019
Line 4,14	0.0018	Line 5,8	0.0016	Line 5,6	0.0004
Line 6,11	0.0011	Line 7,8	0.0006	Line 8,9	0.0051
Line 10,11	0.0006	Line 10,13	0.0006	Line 10,32	0.0700
Line 12,13	0.0061	Line 13,14	0.0014	Line 14,15	0.0030
Line 16,17	0.0012	Line 16,19	0.0027	Line 16,21	0.00019
Line 17,18	0.0011	Line 17,27	0.0024	Line 19,33	0.0560
Line 20,34	0.0420	Line 21,22	0.0020	Line 22,23	0.0013
Line 23,24	0.0049	Line 23,36	0.0140	Line 25,26	0.0045
Line 26,27	0.0021	Line 26,28	0.0066	Line 26,29	0.0088
Line 29,38	0.0700	Line 6,31	0.0840	Line 19,20	0.0019
Line 2,25	0.0012	Line 11,12	0.0061	Line 22,35	0.0280
Line 4,5	0.0018	Line 15,16	0.0013	Line 25,37	0.0140
Line 6,7	0.0013	Line 16,24	0.0008	Line 28,29	0.0021
Line 9,39	0.0280				

All line impedances in scenario c) are 0.6 times the value in TABLE E. I

TABLE E. II
TERMINAL VOLTAGES AND ACTIVE POWER OUTPUTS OF NINE CIGS UNDER DIFFERENT SCENARIOS OF ACTUAL OPERATING CONDITIONS (PER-UNIT)

Scenarios	Operating conditions	
a)	P	1.000,0.973,0.952,0.942,0.922,0.871,0.851,0.892,0.601
	U	0.932,0.924,0.936,0.944,0.900,0.907,0.913,0.929,0.915
b)	P	1.000,0.952,0.902,0.851,0.921,0.871,0.851,0.802,0.601
	U	0.932,0.923,0.938,0.945,0.902,0.910,0.912,0.922,0.916
c)	P	1.000,0.900,0.800,0.700,0.600,0.500,0.400,0.300,0.200
	U	1.032,1.029,1.036,1.039,1.005,1.012,1.016,1.019,1.023

From left to right, terminal voltages and active power outputs of CIG1-CIG9 are listed in sequence

APPENDIX D

Detailed Expression of $\boldsymbol{G}(s)$, $\bar{\boldsymbol{G}}(s)$, and $\bar{\boldsymbol{\Lambda}}(s)$ in Section VI.C

The detailed expression of $\boldsymbol{G}(s)$ and $\bar{\boldsymbol{G}}(s)$ in Section VI.C are

$$\boldsymbol{G}(s)=p_{11}\hat{\boldsymbol{Y}}_{\mathrm{CIG1}}(s)+p_{12}\hat{\boldsymbol{Y}}_{\mathrm{CIG2}}(s)+p_{13}\hat{\boldsymbol{Y}}_{\mathrm{CIG3}}(s)=\begin{bmatrix}G_{11}(s) & 0\\ 0 & G_{22}(s)\end{bmatrix} \quad (43)$$

where

$$\begin{cases}G_{11}(s)=\sum_{i=1}^{3}\dfrac{p_{1i}U_iH_{\mathrm{C}}(s)G_{\mathrm{APC}}(s)}{\left(sL_{\mathrm{f}}+H_{\mathrm{C}}(s)\right)+U_iH_{\mathrm{C}}(s)G_{\mathrm{APC}}(s)}\\ G_{22}(s)=-\sum_{i=1}^{3}\dfrac{p_{1i}U_iH_{\mathrm{C}}(s)H_{\mathrm{pll}}(s)}{\left(sL_{\mathrm{f}}+H_{\mathrm{C}}(s)\right)\left(1+U_iH_{\mathrm{pll}}(s)\right)}\end{cases}$$

The detailed expression of $\bar{\boldsymbol{G}}(s)$ in Section VI.C are

$$\bar{\boldsymbol{G}}(s)\approx\begin{bmatrix}\dfrac{U_{eq}G_{\mathrm{APC}}(s)}{1+U_{eq}G_{\mathrm{APC}}(s)} & 0\\ 0 & -\dfrac{U_{eq}H_{\mathrm{pll}}(s)}{1+U_{eq}H_{\mathrm{pll}}(s)}\end{bmatrix}=\begin{bmatrix}\dfrac{0.9s^2+7.2s}{0.038s^3+0.9s^2+7.2s} & \\ & \dfrac{-4.05s^3-6480s^2}{s^4+4.05s^3+6480s^2}\end{bmatrix} \quad (44)$$

The detailed expression of $\bar{\boldsymbol{\Lambda}}(s)$ in Section VI.C are

TABLE E. III
PARAMETERS OF A PRACTICAL POWER SYSTEM WITH HIGH WIND PENETRATION IN CHINA (PER-UNIT)

Parameters of the PLL-Based Control					
PI parameters of the current control loop: 1.30, 130.07(Regions ① and ②) 1.56, 86.72 (Regions ③, ④, and ⑤)					
PI parameters of DC voltage control loop: 4.18, 16.71(Regions ① and ②) 3.76, 27.84 (Regions ③, ④, and ⑤)					
DC capacitance and base voltage of dc bus: 0.1089, 1					
PI parameters of the PLL: 50, 18000 (Regions ① and ②) 84, 24500 (Regions ③, ④, and ⑤)					
Filter inductance: 0.1225					
Rated capacity of converters: 1					
Parameters of Network Topology					
Parameter	Value	Parameter	Value	Parameter	Value
$Line_{55,86}$	0.00016	$Line_{56,86}$	0.00058	$Line_{57,86}$	0.00157
$Line_{58,86}$	0.00219	$Line_{59,86}$	0.00189	$Line_{60,86}$	0.00132
$Line_{61,86}$	0.00113	$Line_{62,86}$	0.00096	$Line_{63,87}$	0.00059
$Line_{64,87}$	0.00208	$Line_{65,87}$	0.00155	$Line_{66,87}$	0.00125
$Line_{67,87}$	0.00096	$Line_{68,87}$	0.00023	$Line_{69,87}$	0.00010
$Line_{70,87}$	0.00033	$Line_{71,88}$	0.00190	$Line_{72,88}$	0.00160
$Line_{73,88}$	0.00169	$Line_{74,88}$	0.00146	$Line_{75,88}$	0.00101
$Line_{76,88}$	0.00087	$Line_{77,88}$	0.00054	$Line_{78,90}$	0.00013
$Line_{79,90}$	0.00146	$Line_{80,89}$	0.00013	$Line_{81,89}$	0.00146
$Line_{82,91}$	0.00101	$Line_{83,91}$	0.00087	$Line_{84,91}$	0.00101
$Line_{85,91}$	0.00087	$Line_{86,87}$	0.00461	$Line_{89,90}$	0.00461
$Line_{87,92}$	0.00693	$Line_{88,92}$	0.00289	$Line_{90,92}$	0.00520
$Line_{91,92}$	0.00058	$Line_{92,93}$	0.00470		
The boost transformers' impedance of the converters=0.067					

The impedances of all lines in scenario a) are 1.08 times the value in TABLE E. III. $Line_{92,93}$ in scenario b) is 0.00530.

TABLE E. IV
TERMINAL VOLTAGES AND ACTIVE POWER OUTPUTS OF 54 CIGS UNDER DIFFERENT SCENARIOS OF ACTUAL OPERATING CONDITIONS (PER-UNIT)

Scenarios	Operating conditions	
a)	*P*	1.000,0.995,0.990,0.975,0.820,0.765,0.735,0.985,0.980 0.870.0.965,0.960,0.825,0.950,0.975, 0.770,0.935,0.930 0.925,0.920,0.915,0.910,0.905,0.900,0.895,0.890,0.885 0.880,0.875,0.970,0.865,0.860,0.855,0.850,0.845,0.840 0.835,0.830, 0.955,0.815,0.810,0.805,0.8000.795,0.790 0.785,0.780,0.775, 0.940,0.760,0.755,0.750,0.745,0.740
	U	0.9202,0.9203,0.9203,0.9204,0.9211,0.9213,0.9215,0.9201,0.9201, 0.9203,0.9203,0.9204,0.9205,0.9165,0.9205,0.9205,0.9166,0.9166, 0.9166,0.9166,0.9167,0.9167,0.9167,0.9167,0.9167,0.9168,0.9168 0.9168,0.9168,0.9532,0.9532,0.9534,0.9534,0.9534,0.9535,0.9535 0.9535,0.9536,0.9495,0.9496,0.9496,0.9496,0.9496,0.9484,0.9485 0.9485,0.9485,0.9485,0.9549,0.9549,0.9550,0.9550,0.9550,0.9551
b)	*P*	0.979,0.969,0.959, 0.870,0.622,0.513,0.454,0.949,0.939 0.721,0.909,0.899, 0.632,0.880, 0.929, 0.523 ,0.850,0.840 0.830,0.820,0.810,0.800,0.790,0.781,0.771,0.761,0.751 0.741,0.731, 0.919,0.711,0.701,0.691,0.681,0.672,0.662 0.652,0.642, 0.889,0.612,0.602,0.592,0.583,0.573,0.563 0.553,0.543,0.533, 0.860,0.503,0.493,0.484,0.474,0.464
	U	0.9504,0.9505,0.9505,0.9507,0.9519,0.9523,0.9524,0.9503,0.9503 0.9506,0.9506,0.9507,0.9508,0.9462,0.9509,0.9510,0.9462,0.9462 0.9463,0.9464,0.9465,0.9465,0.9466,0.9466,0.9467,0.9467,0.9468 0.9468,0.9468,0.9766,0.9766,0.97670.9767,0.9768,0.9768,0.9769 0.9769,0.9769,0.9748,0.9748,0.9749,0.9749,0.9749,0.9743,0.9743 0.9744,0.9744,0.9744,0.9775,0.9776,0.9776,0.9776,0.9777,0.9778
c)	*P*	1.000,0.999,1.000, 0.971,0.881,0.852,0.832,0.990,0.989 0.920,0.979,0.981, 0.891,0.970, 0.991,0.849,0.959,0.961 0.951,0.949,0.951,0.941,0.940,0.942,0.931,0.930,0.932 0.921,0.920, 0.980,0.910,0.909,0.911,0.900,0.899.0.901 0.890,0.889, 0.970,0.879,0.881,0.870,0.869,0.871,0.860 0.859,0.861,0.850, 0.960,0.840,0.839,0.841,0.830,0.829
	U	0.9098,0.9098,0.9097,0.9098,0.9105,0.9106,0.9107,0.9095,0.9095 0.9098,0.9098,0.9097,0.9099,0.9025,0.9099,0.9100,0.9024,0.9023 0.9024,0.9025,0.9026,0.9026,0.9026,0.9026,0.9027,0.9028,0.9027 0.9028,0.9028,0.9493,0.9494,0.9495,0.9495,0.9495,0.9496,0.9496 0.9497,0.9497,0.9450,0.9451,0.9451,0.9451,0.9451,0.9435,0.9436 0.9436,0.9436,0.9435,0.9509,0.9509,0.9510,0.9509,0.9509,0.9511

Terminal voltages and active power outputs of CIG1-CIG54 are listed in sequence

ACKNOWLEDGMENT

We greatly appreciate Professor Fei Teng from Imperial College London for his important suggestions on this paper.

REFERENCES

[1] D. Koraki and K. Strunz, "Wind and solar power integration in electricity markets and distribution networks through service-centric virtual power plants," *IEEE Trans. Power Syst.*, vol. 33, no. 1, pp. 473–485, Jan. 2018.

[2] T. Jiang, P. Ju, C. Wang, et al., "Coordinated control of air-conditioning loads for system frequency regulation," *IEEE Trans. Smart Grid*., vol. 12, no. 1, pp. 548-560, 2020.

[3] Power System Dynamic Performance Committee, "Stability definitions and characterization of dynamic behavior in systems with high penetration of power electronic interfaced technologies," *IEEE Trans. Power Syst.*, vol. 11, no. April, pp. 2108–2117, 2020.

[4] N. Hatziargyriou et al., "Definition and Classification of Power System Stability – Revisited & Extended," *IEEE Trans. Power Syst.*, vol. 36, no. 4, pp. 3271-3281, July 2021.

[5] Y. Chen, L. Xu, A. Egea-Àlvarez and B. Marshall, "Accurate and General Small-Signal Impedance Model of LCC-HVDC in Sequence Frame," *IEEE Trans. Power Deliv.*, doi: 10.1109/TPWRD. 2023.3307552.

[6] B. Wen, D. Dong, D. Boroyevich, et al., "Impedance-based analysis of grid-synchronization stability for three-phase paralleled converters," *IEEE Trans. Power Electron.,* vol. 31, no. 1, pp. 26-38, 2015.

[7] W. Du, W. Dong, and H. Wang, "A method of reduced-order modal computation for planning grid connection of a large-scale wind farm," *IEEE Trans Sustain Energy.,* vol. 11, no. 3, pp. 1185-1198, 2019.

[8] H. Liu, X. Xie, J. He, et al., "Subsynchronous interaction between direct-drive PMSG based wind farms and weak AC networks," *IEEE Trans. Power Syst.,* vol. 32, no. 6, pp. 4708-4720, 2017.

[9] J. Liu et al., "Impact of Power Grid Strength and PLL Parameters on Stability of Grid-Connected DFIG Wind Farm," *IEEE Trans Sustain Energy.,* vol. 11, no. 1, pp. 545-557, Jan. 2020,

[10] L. P. Kunjumuhammed, B. C. Pal, C. Oates, et al., "Electrical oscillations in wind farm systems: Analysis and insight based on detailed modeling," *IEEE Trans Sustain Energy.,* vol. 7, no. 1, pp. 51-62, 2015.

[11] J. Quintero, V. Vittal, G. T. Heydt, et al., "The Impact of Increased Penetration of Converter Control-Based Generators on Power System Modes of Oscillation," *IEEE Trans. Power Syst.*, vol. 29, no. 5, pp. 2248-2256, Sept. 2014,

[12] "Reliability guideline: Integrating inverter-based resources into weak power systems," *North Amer. Elect. Rel. Corporation*, Jun. 2017. [Online]. Available: http://www.nerc.com/pa/RAPA/rg/ReliabilityGuidelines.

[13] Australian Energy Market Operator. (2018, Jun.). "System strength impact assessment guidelines," https://www.aemo.com.au/-/media/files/electricity/nem/security_and_reliability/system-security-market-frameworks-review/2018/system_strength_impact_assessment_guidelines_published.pdf.

[14] Australian Energy Market Operator. (2020, Oct.). "Investigation into system strength frameworks in the NEM," https://www.aemc.gov.au/sites/default/files/2020-10/System%20strength%20investigation%20-%20final%20report%20-%20for%20publication.pdf.

[15] Y. Zhang, S. H. Huang, J. Schmall, et al., "Evaluating system strength for large-scale wind plant integration," in *Proc. IEEE Power Energy Soc. Gen. Meeting*, Jul. 2014, pp. 1–5.

[16] R. Fernandes, S. Achilles, and J. MacDowell, "Minnesota Renewable Energy Integration and Transmission Study Final Report," GE Energy Consulting, Schenectady, NY, USA, Oct. 2014. [Online]. Available: http://www.minnelectrans.com/documents/MRITS-report.pdf.

[17] CIGRE Working Group B4.62, "Connection of wind farms to weak AC networks," TGS, CIGRE WG B4-62, 2017.

[18] IEEE Standard for Interconnection and Interoperability of Inverter-Based Resources (IBRs) Interconnecting with Associated Transmission Electric Power Systems, IEEE Standard 2800™-2022, 2022.

[19] H. Yuan, H. Xin, D. Wu, et al., "Assessing Grid-Accommodable Renewable Capacity with Small-signal Stability Constraints". TechRxiv, 20-Jan-2022.

[20] F. Zhang, H. Xin, D. Wu, et al., "Assessing Strength of Multi-Infeed LCC-HVDC Systems Using Generalized Short-Circuit Ratio," *IEEE Trans. Power Syst*., vol. 34, no. 1, pp. 467-480, Jan. 2019.

[21] W. Dong, H. Xin, D. Wu, et al., "Small Signal Stability Analysis of Multi-Infeed Power Electronic Systems Based on Grid Strength Assessment," *IEEE Trans. Power Syst*., vol. 34, no. 2, pp. 1393-1403, March 2019.

[22] H. Xiao and Y. Li, "Multi-Infeed Voltage Interaction Factor: A Unified Measure of Inter-Inverter Interactions in Hybrid Multi-Infeed HVDC

Systems," *IEEE Trans. Power Deliv.,* vol. 35, no. 4, pp. 2040-2048, Aug. 2020.
[23]H. Xiao, Y. Zhang, X. Duan, et al., "Evaluating Strength of Hybrid Multi-Infeed HVDC Systems for Planning Studies Using Hybrid Multi-Infeed Interactive Effective Short-Circuit Ratio," *IEEE Trans. Power Syst*., vol. 36, no. 4, pp. 2129-2144, Aug. 2021.
[24]L. Fan, "Modeling type-4 wind in weak grids," *IEEE Trans. Sustain. Energy*, vol. 10, no. 2, pp. 853-864, Apr. 2019.
[25]L. Huang, H. Xin and F. Dörfler, "H∞-Control of Grid-Connected Converters: Design, Objectives and Decentralized Stability Certificates," *IEEE Trans. Smart Grid.*, vol. 11, no. 5, pp. 3805-3816, Sept. 2020.
[26]L. Fan and Z. Miao, "An explanation of oscillations due to wind power plants weak grid interconnection," *IEEE Trans. Sustain. Energy*, vol. 9, no.1, pp. 488–490, Jan. 2018.
[27]R. Burgos, D. Boroyevich, F. Wang, et al, "On the ac stability of high power factor three-phase rectifiers," in *Proc. Energy Convers. Congr. Expo.,* Sep. 2010, pp. 2047–2054.
[28]B. Wen, R. Burgos, D. Boroyevich, et al, "AC Stability Analysis and dq Frame Impedance Specifications in Power-Electronics-Based Distributed Power Systems," *IEEE Journal of Emerging and Selected Topics in Power Electronics*, vol. 5, no. 4, pp. 1455-1465, Dec. 2017.
[29]J. Kevorkian and J. D. Cole, *Multiple Scale and Singular Perturbation Methods*, vol. 114, Brelin, Germany: Springer, Sep. 2012.
[30]C. Yang, Z. Gong, M. Hong, et al, "Applicability Analysis of the Generalized-impedance Stability Criterion for Converters Considering the Outer-loop Dynamics," (in Chinese) *Proc. CSEE*, vol. 41, no. 9, pp: 3012-3023, May 2021.
[31]ICS National Standard of the People's Republic of China, "Technical specification for connecting wind farm to power system—Part 1: On shore wind power", GB/T 19963.1-2021, 2021.
[32]P.C.S.Krishayya, R.Adapa, M.Holm, et al, "IEEE guide for planning DC links terminating at AC locations having low short-circuit capacities, Part I: AC/DC system interaction phenomena", France: CIGRE, 1997.
[33]G. W. Stewart, "Matrix perturbation theory", 1990.
[34]R. Horn and C. Johnson, Matrix Analysis. Cambridge, U.K.: Cambridge Univ. Press, 1985.

Chenxi Liu received the B.Eng. degree in Electrical and Electronic Engineering, North China Electric Power University, Beijing, China, in 2020. She is currently working toward the Ph.D. degree in the College of Electrical Engineering, Zhejiang University, Hangzhou. Her research interests include renewable power system stability analysis and control.

Huanhai Xin received the Ph.D. degree in the College of Electrical Engineering, Zhejiang University, Hangzhou, China, in June 2007. He was a postdoctoral researcher in the Department of Electrical Engineering and Computer Science, University of Central Florida, Orlando, USA, from June 2009 to July 2010. He is currently a Professor in the College of Electrical Engineering, Zhejiang University. He is currently supported by the National Natural Science of China for Excellent Young Scholars. His research interests include renewable power system stability analysis and control.

Di Wu (M'14) received a Ph.D. degree in the area of applied complex networks from Polytechnic University of Turin, Italy, in 2011. He also holds another Ph.D. degree in the area of power system engineering obtained from Zhejiang University, China. His M.S. and B.S. degrees in electrical engineering were obtained from Zhejiang University and Kunming University of Science and Technology, China, in 2005 and 2002, respectively. Dr. Wu is currently an Associate Professor in the Department of Electrical and Computer Engineering at North Dakota State University. His research interests include renewable energy integration, power system dynamics and stability, cascading failures, and the application of complex network theory in power grids.

Huisheng Gao received his Ph.D. degree in the College of Electrical Engineering at Zhejiang University in 2022, and a B.Eng. degree from Zhejiang University in 2017. Currently, he is a post-doctor with the College of Electrical Engineering at Zhejiang University. His research interests include frequency stability analysis and control in renewable-integrated power systems.

Hui Yuan received the B. Eng. degree from the College of Automation, Wuhan University of Technology, Wuhan, China, in 2013, M. Eng. degree from the College of Electrical Engineering, Guangxi University, Nanning, China, in 2016, and Ph. D. degree from the College of Electrical Engineering, Zhejiang University, Hangzhou, China, in 2021, respectively. He is currently working as post-doctor in the College of Electrical Engineering, Zhejiang University. His research interests include renewable power system stability analysis and control.

Yuhan Zhou received the B.Eng. degree in Electrical and Electronic Engineering, North China Electric Power University, Beijing, China, in 2019. He is currently working toward the Ph.D. degree in the College of Electrical Engineering, Zhejiang University, Hangzhou. His research interests include renewable power system stability analysis and control.